Journal of Modern Optics
Vol. 55, No. 13, 20 July 2008, 2141–2177

Taylor & Francis
Taylor & Francis Group

Characterization of the supercontinuum radiation generated by self-focusing of few-cycle 800 nm pulses in argon

Kyriaki Kosma, Sergei A. Trushin, Werner Fuß*
and Wolfram E. Schmid

Max-Planck-Institut für Quantenoptik, Garching, Germany

(*Received 5 November 2007; final version received 8 February 2008*)

Self-focusing of few-cycle pulses in atmospheric-pressure argon results in a supercontinuum which differs remarkably from the case of longer pulses: under single-filament conditions it extends to 200 nm and 250 nm with 6 fs and 10 fs pulses, respectively; the radiation, including the shortest wavelengths, is collimated and shows no conical emission. The short-wavelength part is intrinsically at least as short as the incoming fundamental pulse. These features make the few-cycle supercontinuum attractive as a source of a widely tunable 10 fs pump pulses for spectroscopic applications. We present extensive experimental results including the dependence of the spectrum on pulse energy, duration and chirp, filament length, gas pressure and a comparison with nitrogen and air. We discuss them and other features including the role of the third harmonic and identify the conditions required to get a single highly stable filament. We also present a model, based on self-guiding, which predicts useful scaling rules.

Keywords: filamentation; self-phase modulation; self-guiding; chirp effects; tunable short UV pulses

1. Introduction

Propagation of femtosecond pulses in air and other gases is recently much investigated (for reviews, see [1–4]), in particular since the availability of femtosecond lasers. Self-phase modulation (SPM), induced by the Kerr effect (refractive index change $\Delta n_{\mathrm{Kerr}} = n_2 I$, proportional to the time-dependent intensity $I(t)$), phase-modulates the pulses, introducing new frequencies with a temporal chirp. This technique is widely used in combination with a chirped-mirror compressor to generate pulses with durations down to a few cycles [5]. For this purpose, high-power pulses are focused into a gas; to extend the length of interaction at high intensity, it is common practice to guide the wave in a gas-filled capillary [6]. It was recently demonstrated that with several hundred microjoules, simple focusing into argon is sufficient and the capillary can be omitted [7–11], a method that has become popular. Under these conditions one also observes self-focusing and self-guiding (*filamentation*): due to the spatial profile of $I(t, r)$, the same term $n_2 I$ causing SPM also

*Corresponding author. Email: w.fuss@mpq.mpg.de

ISSN 0950–0340 print/ISSN 1362–3044 online

DOI: 10.1080/09500340801979325
http://www.informaworld.com

gives rise to a focusing lens. If the laser power is above a critical value of $P_{cr} = \lambda^2/2\pi n_2$, the beam would totally collapse; this is prevented, however, by a defocusing effect of electrons near the beam axis, produced by ionization at the high intensities. This plasma is usually visible as a luminescing channel (*filament*). In this way (but with terawatt powers), very long 'self-foci' have been produced in air, which has a potential for atmospheric monitoring (e.g. [12–14]).

In applying simple focusing of few-cycle 800 nm pulses into argon, we noticed a pedestal in the spectrum which extends unusually far into the UV, farther than with longer pulses and farther than predicted by simple Kerr-effect SPM theory; some results were briefly communicated [8]. Here we report more details and additional results. The spectrum reaches as far as 200 nm, if the initial pulses are short enough (5–6 fs) [15]. The spectrum can also be broadened by extending the interaction length at high intensity (lengthening the filament), e.g. by choosing a longer focal length (in the case of long pulses). It is worth noting that spectra of comparable width have previously only been obtained with much higher energies or powers [16–19], under conditions where many filaments (*multiple filamentation*) are observed or expected. In addition, much longer propagation lengths were employed. With our smaller energies there is only one filament; in this case, pulse-to-pulse fluctuations are much smaller than with multiple filaments. The broad continuum typically also covers the region of the third harmonic (270 nm). Generation of (isolated) third harmonic radiation has repeatedly been observed by focusing in particular in air (e.g. [18,20–30]), and it was claimed that with growing intensity it merges with the broadening supercontinuum and enhances it [18,25,26]. We present evidence that the third-harmonic contribution to the supercontinuum is negligible under our conditions; a much better yield of the third harmonic is obtained in short gas cells.

2. Experimental

Two different Ti-sapphire laser systems were used in this work. Most experiments were performed with a commercial system (Spectra-Physics Tsunami and Spitfire). It emits pulses at 805 nm with energy of 2 mJ, pulse duration of ≈45 fs (FWHM), spectral half-width of 35 nm (16 THz) at a repetition frequency of 1 kHz. The subsequent setup is shown in Figure 1. To obtain shorter pulses, the beam (initial diameter of $3w = 16$ mm) was attenuated to 0.7–1 mJ (to avoid multiple filamentation) and was focused by a mirror with a focal length of $f = 2$ m into a glass cell, which was typically windowless and 150 cm long, containing slowly flowing argon at ambient pressure (950 mbar). The emerging radiation was recollimated and then three times reflected from chirped mirrors (Layertec, group delay dispersion -120 fs^2). The resulting pulses have a duration of 10–11 fs, measured by an interferometric autocorrelator, and a spectral half-width of 100–110 nm (47–52 THz). Using air instead of Ar results in pulses of 14 fs. After the compression, the pulses were refocused to a second windowless cell with Ar flow, this time by a mirror with $f = 1$ m (sometimes 1.5 m) and a variable diaphragm ('input iris') before the focusing mirror (Figure 1). The spectrum of the emerging radiation was measured by a calibrated broad-band spectrometer (Ocean Optics) covering the range of 1100–200 nm, in some cases by a UV spectrometer (520–200 nm). In most cases, before entering the spectrometer the full beam was spatially integrated by an Ulbricht sphere coated with PTFE. When in

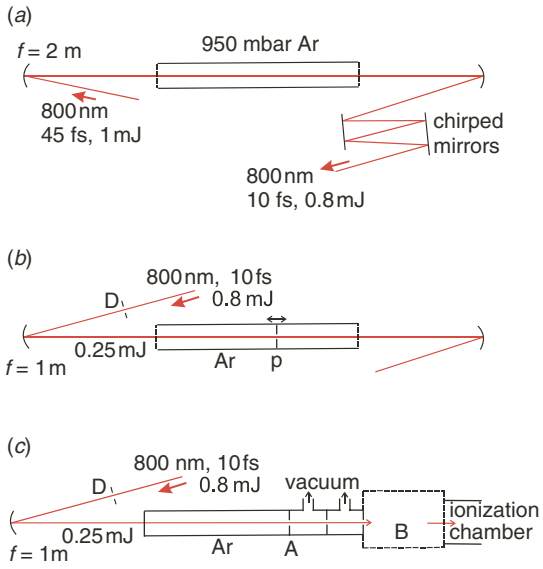

Figure 1. Setup for generation of (*a*) the 10 fs pulses and (*b*) the supercontinuum with atmospheric beam path; the geometrical focus is in the center of the Ar cells; p is an optional pinhole movable along the filament. (*c*) Setup with termination of the filament by an aperture A near the geometrical focus and a vacuum beam path (with differential pumping and additional apertures) beyond A; in the evacuated box B the beam is collimated and focused (dielectric mirrors) to the detection setup (ionization chamber). D is a variable diaphragm (iris). Typical parameters are indicated. (The color version of this figure is included in the online version of the journal.)

contrast the spectral variation over the beam cross-section was to be measured, we used a variable diaphragm before the integrating sphere. The spectra shown in the figures are typically integrated over about 1000 pulses; however, observing single-pulse spectra showed that the shape including the spectral structures are stable from pulse to pulse under conditions, when only a single filament was generated.

For comparison, the spectrum after the first cell (with 45 fs incident pulses) was also investigated, using focal lengths of $f = 1$ and 2 m. In some experiments, the cell was equipped with windows of quartz glass (0.2 mm) or CaF_2 (0.5 mm), so that the pressure could be varied. These cells also served to investigate mixtures of Ar with He.

The other laser system, used in cooperation with A. Baltuška, E. Goulielmakis, F. Krausz, and M. Uiberacker (see also [15]), is based on a commercial unit (Femtolasers: Femtopower Compact Pro), delivering 1 mJ pulses of 25 fs duration at 1 kHz of repetition rate. The pulses are further compressed by SPM in a fused-silica capillary of 1 m length and 0.25 mm diameter, filled with 2 bar of Ne, followed by reflection at chirped mirrors. The resulting pulses had a duration of 5–6 fs and an energy of 0.4 mJ. For further details see [31]. The laser system has a provision to control the carrier envelope phase (Menlo Systems). These pulses were focused into the windowless 1 m cell by a mirror with $f = 1$ m, and the spectrum of the emerging radiation was investigated by the same calibrated spectrometer.

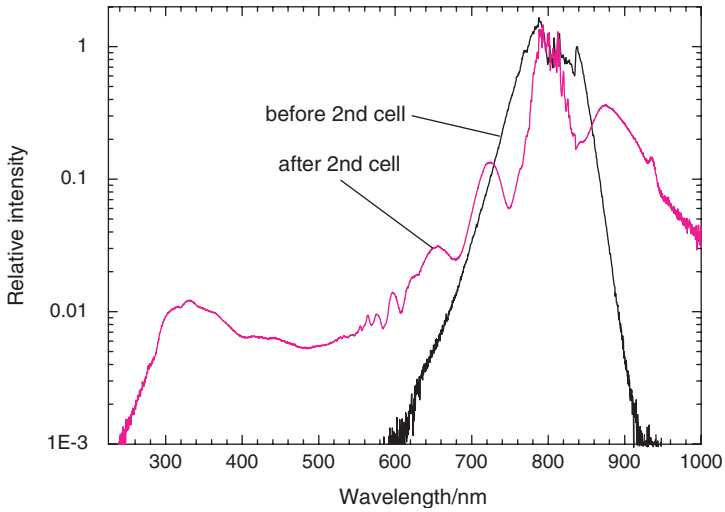

Figure 2. Spectrum ('after 2nd cell') integrated over the output beam under conditions optimized for the maximum of energy in the 300 nm region, i.e. with the iris diameter $d \approx 5$ mm and the incident $E_p = 0.26$ mJ (pulse duration $\tau_p = 10$ fs). A spectrum ('before 2nd cell') of the incident radiation is also displayed for comparison). (The color version of this figure is included in the online version of the journal.)

3. Results

Most measurements have been done with the 10 fs pulses, and we present them first. If a large energy (typically 0.7 mJ, fully opened iris, see the setup in Figure 1) is focused into the Ar cell, a very bright luminescing column of 5–7 cm length is observed at about 10 cm before the geometrical focus. The emerging beam has then a rather poor pointing stability and the spot of transmitted light 'dances'; furthermore, the spectra then show pulse-to-pulse fluctuations of the shape, including the UV cutoff wavelength and the spectral structures. We assume that the beam is broken up under these conditions into multiple filaments. But reducing the input pulse energy E_p by an iris to below a threshold of $E_p = 0.25$–0.35 mJ (iris diameter $d \approx 5$ mm) suddenly gives rise to a fully stable beam. Obviously there is only a single filament under these conditions. The luminescing column is then less bright and is longer ($\approx$15 cm) with its center at $\approx$3–4 cm before the geometrical focus. Under these conditions, 96% of the incident E_p is recovered in the transmitted radiation. Practically all investigations were done with the input iris small enough to obtain a single filament only.

3.1. *Variation of the input iris (input energy) with the 10 fs pulses*

Figure 2 shows a spectrum integrated over the output beam cross-section under conditions optimized for the maximum of energy in the 300 nm region, i.e. with the iris diameter $d \approx 5$ mm and the incident $E_p = 0.26$ mJ. (A spectrum of the incident radiation is also displayed for comparison.) It is fully continuous and extends as far as

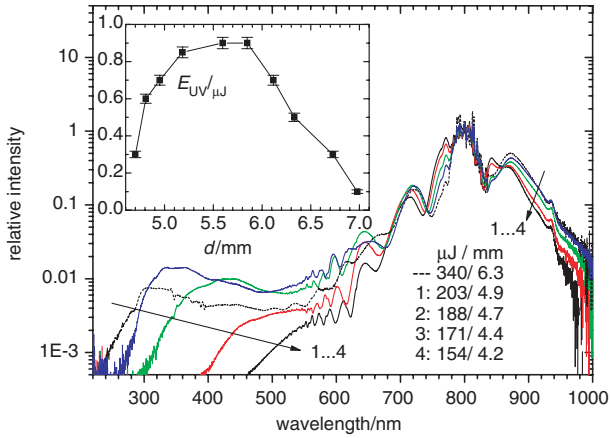

Figure 3. Spectra measured with different iris (diaphragm) diameters d ($\tau_p = 10$ fs). The solid-line spectra are labeled $1 \cdots 4$. The transmitted energies corresponding to the different curves and the d values are compiled in the list. Inset: UV energies, measured as reflected by four dielectric mirrors at 270 nm (bandwidth 19 nm) versus d. (The color version of this figure is included in the online version of the journal.)

250 nm to the UV. In the near IR, it reaches to about 2 μm (not shown), as found by a scanning spectrometer[1]. The general shape of the spectrum including the cutoff and the structures [8] is stable from pulse to pulse. An independent measurement of some spectral parts, using dielectric filters, showed that the UV edge should be lifted by a factor of 2 [8]; probably the calibration curve of the spectrometer is not sufficiently accurate in this region.

The spectra measured with different input iris diameters d are shown in Figure 3 (see also [8]). Obviously the UV part is very sensitive to E_p and/or d. The UV fraction below 300 nm is maximal at $E_p = 0.26$–0.3 mJ; at 0.3 mJ it already shows some instability and decreases rapidly on increasing d (inset of Figure 3; the exact shape of the $E_{UV}(d)$ curve is sensitive to the iris alignment). That is, under conditions of multiple filamentation, there is not only a poor pointing stability and shorter filament (see above) but also less spectral extension to the UV. It is also remarkable that the central part of the spectrum (down to about 10% of the maximum) is not much altered by varying E_p and/or d, despite the strong changes in the pedestal. It is worth noting that multiple filamentation with the longer pulses (45 fs, in the first cell) sets in at about the same power (0.7–1 mJ).

3.2. *Spatial variation of the spectrum (mainly with 10 fs pulses)*

Figure 4 shows a series of spectra obtained when placing an iris of variable diameter (the transmitted energy is indicated in the figure) in the center of the *output beam* before the spectrometer. The input pulses (10 fs) had $E_p = 0.26$ mJ, corresponding to an input iris of $d \approx 5$ mm (as in Figure 2). Closing the output iris practically only reduces the red part of

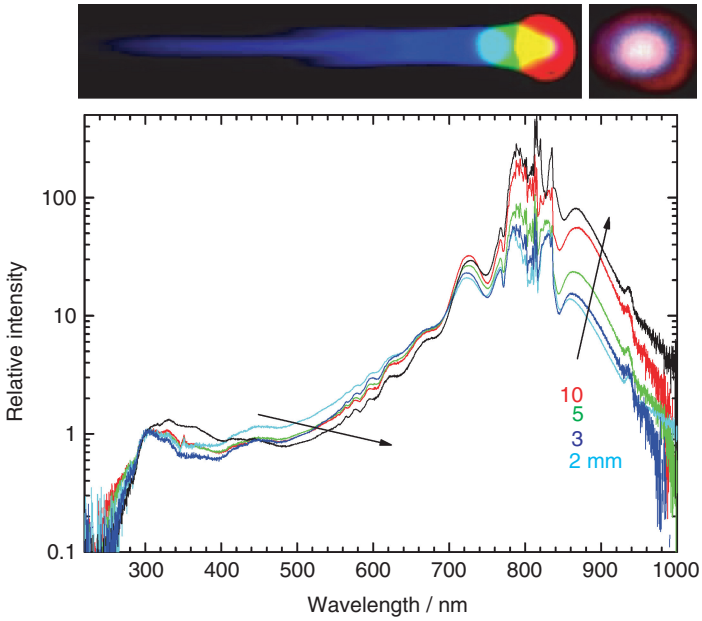

Figure 4. Spatial variation of the spectrum (10 fs) with different diameters of an aperture before the spectrometer. The spectra are normalized at 300 nm. The photograph shows a spectrum, made by dispersion of the collimated beam by a CaF_2 prism; the shortest wavelengths extend to the UV range.

the spectrum. That means that the *blue and UV parts are concentrated on the axis*. This is consistent with the photograph in Figure 4: the part dispersed with a prism indicates that the center of the beam contains all spectral components and extends farthest into the UV range. In the nondispersed photograph, the central spot is surrounded by a red ring, containing about 14% of the energy. This value suggests that this ring is just the second maximum of the Airy pattern caused by the input iris, containing the fundamental wavelength. But according to the spectra in Figure 4, also in the low-intensity wings (down to about 5 or 3 mm of diameter) of the central bell-shaped spot (which can be fitted to a Gaussian with $3w_0 = 10$ mm) the fraction of red light is higher than on the axis. Except this variation of the red fraction, there is nearly no spectral dependence on the diameter at wavelengths shorter than 750 nm; even the modulation remains unchanged. This means that the broadened part of the spectrum is spatially homogeneous (under the condition that the input iris is well aligned, see below).

This is in clear contrast to previous observations with longer pulses: frequently in self-focusing one obtains 'conical emission'; the beam then consists of a central spot surrounded by colored rings (see, e.g. [19,32–36] or the reviews [2,3]), and in many cases most of the energy at the short wavelengths is contained in these rings. In fact, we also noticed this effect with the 45 fs pulses: blue and UV rings and side spots appeared, and spots could be found containing an isolated third harmonic. (Also in [27], using 50 fs pulses, a large part of the third harmonic was found in a ring.) We can conclude that,

if there is also conical emission with the 10 fs pulses, the cone angles are so small that they were not detected.

The spectral distribution in the central spot is circularly symmetric (as in the photograph) only with a careful positioning of the iris before the second gas cell. Displacing the iris sideways (<0.5 mm), the central spot showed a slight horizontal displacement of the UV output (with maximum $\approx$320 nm) versus the red part, and this red part sometimes has a dark center. With such a slight misalignment and with the output iris optimized for maximum UV power, the relative energy in the UV maximum around 320 nm (measured with spatial integration; i.e. without diaphragm before the Ulbricht sphere) is nearly the same as with the best iris position; but the spectral valley between this and the red part is deepened with smaller output iris.

We also determined the beam profile in the *focal region* within the Ar cell by measuring the transmission of pinholes, placed there (Figure 1*b*), as a function of their diameter d_p (see [8]). It can be described by a central bell-shaped part (Gaussian with waist radius $w_0 = 160$ μm, or the central part of an Airy pattern) surrounded by a ring containing 14% of the total energy, as expected for an Airy pattern. Evaluating in the same way the UV transmissions of the pinholes results in a w_0 of 140 μm, by 13% less than for the total radiation. The waist practically coincides with that calculated for focusing a Gaussian beam. Also the length of the focal region agrees with twice the Rayleigh length as in Gaussian optics (see [8]). Only the center of the waist indicates a slight deviation: it is 2–3 cm before the geometrical focus, as expected with self-focusing. A stronger argument that self-focusing does in fact occur is based on the Kerr term $n_2 I(r, t)$, whose t dependence is clearly observed as SPM, so that the spatial (r) dependence should also be present. Extrapolation of the radial intensity profile results in a maximum intensity on the axis of 47 TW cm^{-2}. This is just the same as previously suggested for the maximum ('clamped') intensity in self-focusing in gases [37–39].

3.3. *Variation of the interaction length (10 fs pulses)*

According to [25] propagation of self-focusing can be stopped by cutting the outer wings ('background reservoir') by a pinhole in the filament region. This is explained by the model that the background reservoir is focused to the axis only on further propagation. After blocking this reservoir, the radiation on the axis diverges and is not recollimated. We varied the diameter d_p of the pinhole, placed in the region of the luminescing region, from 400 to 150 μm. The luminescence after the hole was visibly attenuated only below 200 μm and was stopped at $d_p = 150$ μm. Moving the pinhole of this d_p along the propagation direction (z) hence allows one to control the filament length z_{fil}, which is the high-intensity length of interaction with Ar. Figure 5(*a*) shows the transmission of the pinhole as a function of z, measured for the full spectrum and for the UV part around 270 nm (filtered by reflection from two dielectric mirrors, effective halfwidth 19 nm); before insertion of the pinhole, the input iris was optimized for maximum UV yield. Over a region of z, where the total energy stays practically constant, the UV energy keeps increasing, reaching a maximum at a position ($D = 103$–105 cm) where the filament would also terminate without a pinhole. Figure 5(*b*) shows how the UV spectra evolve with the pinhole position: the cutoff is steadily pushed to shorter wavelengths on increasing z again

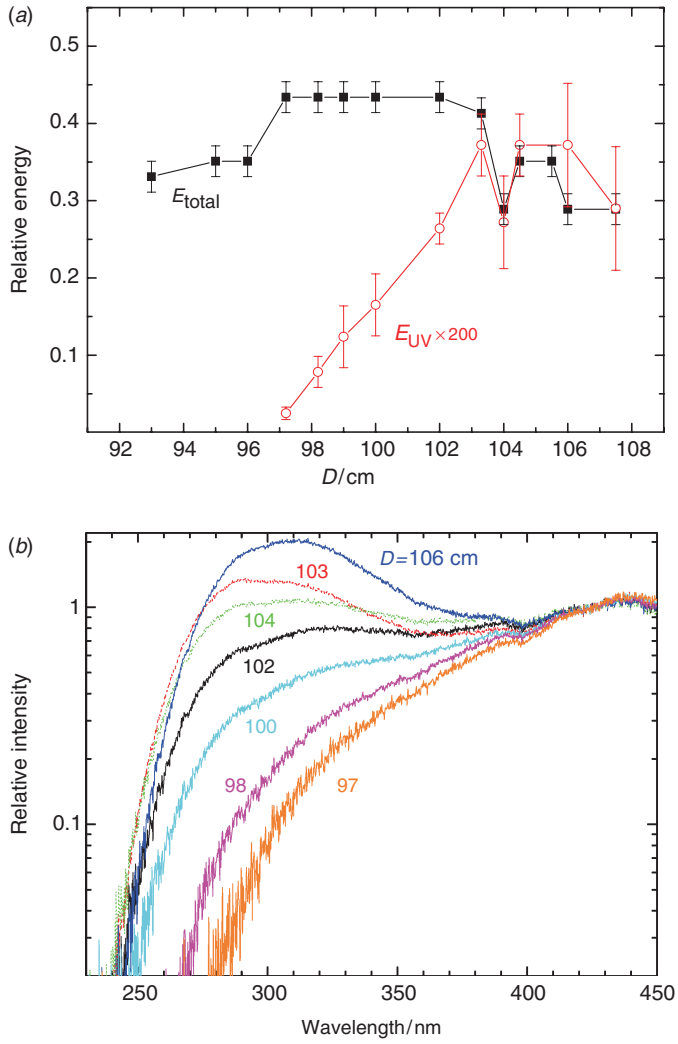

Figure 5. (*a*) Transmission of the 150 μm pinhole as a function of its distance *D* from the focusing mirror, measured for the full spectrum and for the UV part around 270 nm. (*b*) Evolution of the UV spectrum (normalized at 430 nm) with the pinhole position *D*. (Note: a similar figure in [15] shows a corrupted wavelength scale with numbers of 200–550 nm instead of 250–550 nm.) (The color version of this figure is included in the online version of the journal.)

to $D \approx 104$ cm. (Note: in a similar figure shown in [15], the wavelength scale is corrupted, indicating a range of 200–550 nm instead of 250–550 nm.)

3.4. *Effect of the focal length (10 fs and 45 fs pulses)*

Figure 6(*a*) compares the spectra obtained with $f = 1$ m (conditions as in Figure 2) and $f = 1.5$ m, using the 10 fs pulses. The difference is only marginal. By contrast, a very

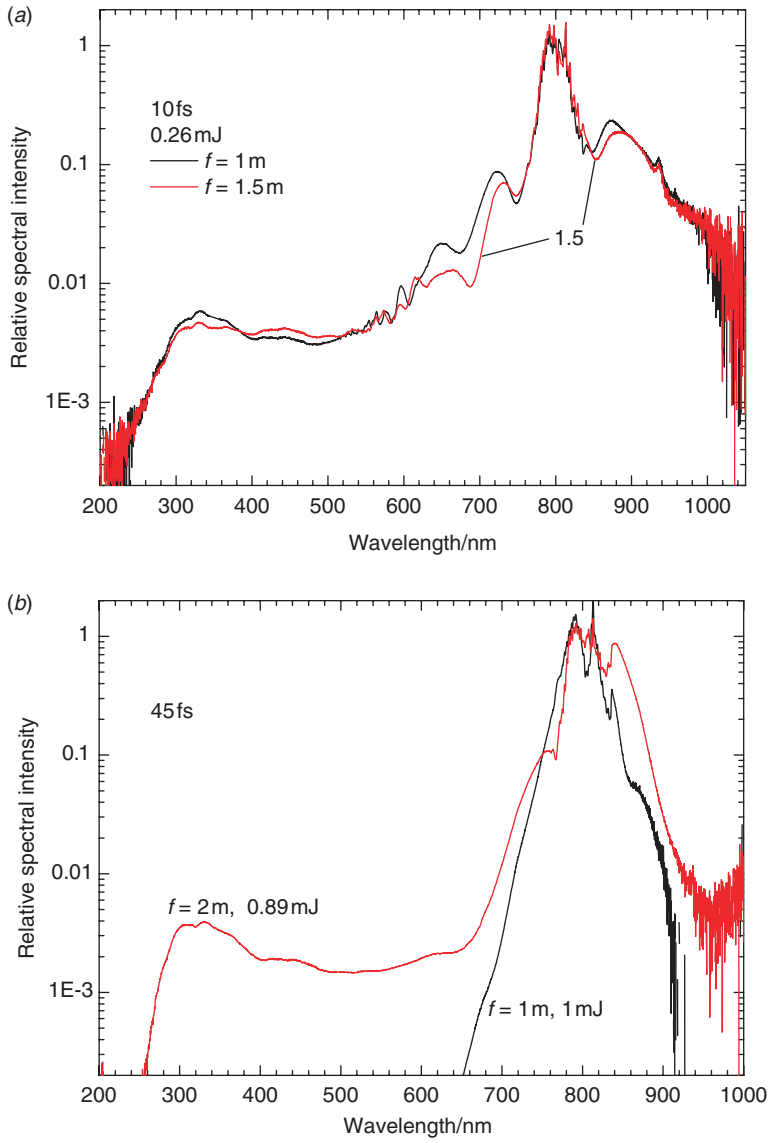

Figure 6. (*a*) Spectra obtained with $f = 1$ m (conditions as in Figure 2) and $f = 1.5$ m, using the 10 fs pulses. (*b*) Spectra with $f = 1$ and 2 m, using the 45 fs pulses. (The color version of this figure is included in the online version of the journal.)

pronounced effect was obtained with the 45 fs pulses (Figure 6(*b*)): with $f = 2$ m the spectrum (spatially integrated by the Ulbricht sphere) reaches to 250 nm (with most of the short-wavelength part contained in conical emission) however, as far as with the 10 fs pulses (that show no conical emission, see Section 3.2) at $f = 1$ m. (Note that the chirped mirrors, used before entering the second cell, cut away the pedestal, as shown by the spectrum before the second cell in Figure 2.) As judged by the eye, z_{fil} increases in this case

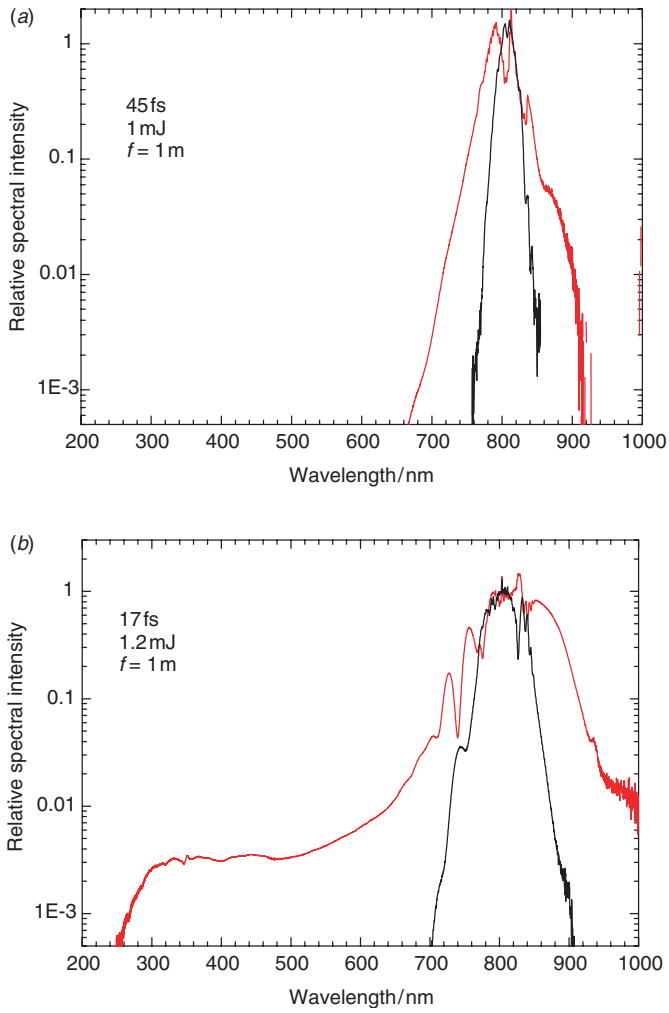

Figure 7. (*a*)–(*c*) Comparison of the input with the output spectra for the pulse durations 45, 17 and 6 fs, focusing with focal length $f = 1$ m into Ar (10 fs: see Figure 2); the Ar pressure was 950 mbar, except for the 17 fs pulses, where a mixture of 250 mbar Ar + 700 mbar He was used. (*d*) Output spectra for different pulse durations. (The color version of this figure is included in the online version of the journal.)

with the focal length. It is also worth noting that the halfwidth does not change with f, although the cutoff wavelength does in the case of the longer pulses.

3.5. *Effect of pulse duration*

Figures 7(*a*)–(*c*) compares the input with the output spectra for the pulse durations 45, 17 and 6 fs, focusing into 950 mbar of Ar by $f = 1$ m; the corresponding data for 10 fs have already been shown in Figure 2. The data for 17 fs are from [40] and those

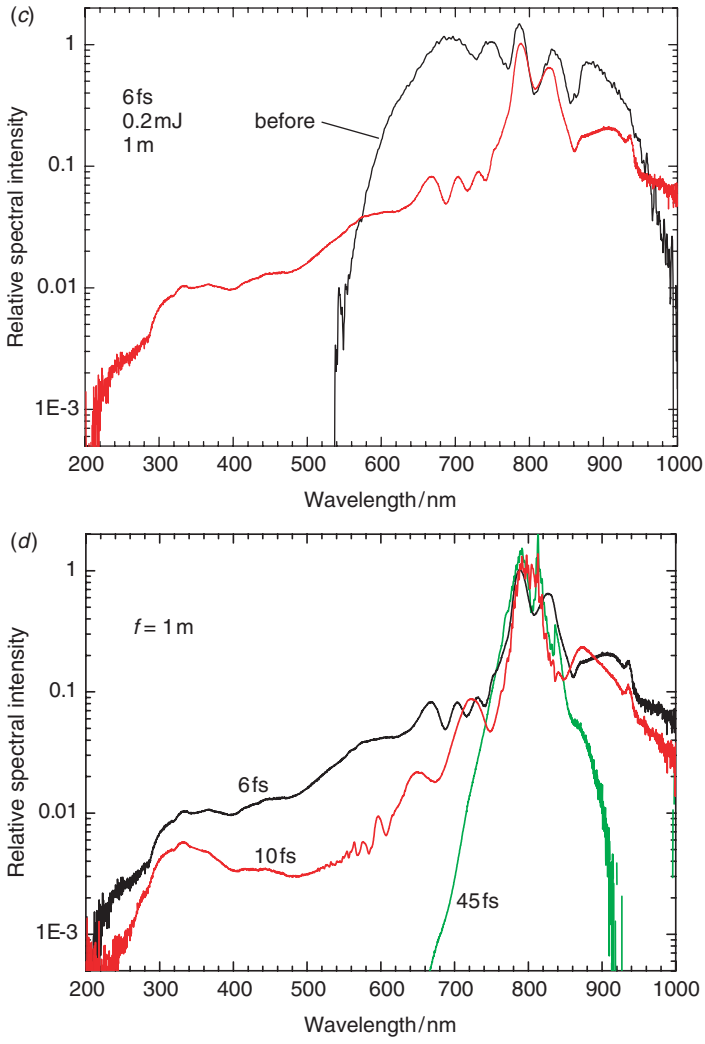

Figure 7. Continued.

for 6 fs from [15]. The powers were not much different (22, 24 and 30 GW, the latter value applying also to 10 fs). It is obvious that with this focal length a broad pedestal only appears with the shorter pulses. It is the broader and more intense, the shorter the pulses; the output spectra are compared in Figure 7(*d*), some results of which have already been separately reported [15]. It is surprising that the half-widths seem to behave the other way around: whereas the 45 fs pulses are broadened from 30 to 100 nm (full width at half maximum, FWHM) by passing through the Ar cell, the 10 fs pulses are narrowed: the FWHM decreases from 100 to 50 nm (47 to 23 THz), although the effect would be smaller, if the spectral modulation were smoothed (Figure 2). But with the 6 fs pulses the narrowing is very pronounced (from 250 to 70 nm). This is particularly

remarkable, because the initial width is about 1.6 times bandwidth limited. Spectral narrowing therefore also implies substantial pulse lengthening (in the transform limit to 13 fs). On the other hand, the 17 fs data show a broadening of both, the half-width (100 nm) and the pedestal. It turned out that the half-width is sensitive to an initial chirp (see Section 3.6). In the data reported so far, the input pulse parameter's energy (varied by the input iris) and also the chirp – which was not measured – were optimized for the shortest-wavelength UV output. An interesting observation in Figure 7(*d*) is that if the spectral modulations are smoothed out a little, the spectra practically coincide in the range down to about 10% of the maximum, although the pedestals and UV cutoffs drastically differ for the three pulse durations.

As already communicated in [15], with the 6 fs pulses we also investigated whether the carrier-envelope phase has any influence. This phase was stabilized in such a way that the pulses are either cosine or sine pulses. (The former has a single amplitude maximum at the maximum of the envelope, the latter has two equal amplitude maxima.) But the spectrum in the investigated range turned out to be not sensitive to this phase.

3.6. *Influence of an initial chirp (45 fs and 10 fs pulses)*

The chirp influence on supercontinuum generation was mainly investigated with the 45 fs pulses. For this purpose, we varied the distance of the retroreflector from the grating in the compressor of the laser system. The input iris (diameter 5 mm) and energy was kept constant at the value that is optimum for UV generation at chirp zero. A convenient indirect measure of the chirp is the pulse duration; it is indicated in Figure 8(*a*) (45 fs or longer) as the abscissa and in Figure 8(*b*) (10 fs or longer) as a parameter. Figure 8(*a*) shows that for the 45 fs pulses the halfwidth after focusing ($f = 2$ m) through the Ar cell strongly depends on the chirp: if it is negative, the region near the fundamental becomes narrower, but it is broadened if the chirp is positive. The total variation is by a factor of 9. The largest and smallest bandwidths would support pulse durations of 6 and 55 fs in the transform limit. It is also remarkable that to obtain a maximal halfwidth requires a different chirp from that for reaching the broadest pedestal (shortest-wavelength cutoff). The latter is obtained with chirp zero, i.e. with the shortest pulses.

Much less influence of a chirp was observed with the 10 fs pulses (Figure 8(*b*)). It was varied by changing the number of reflections from chirped mirrors and by inserting an optical window. In contrast to the 45 fs pulses, in this case each time the input iris and other alignments were optimized for the best UV yield. But it seems clear that with suitable optimization of the input parameters (energy and iris, probably a positive chirp), the halfwidth can also be increased. This is obviously necessary for further compressing the pulses, as done in [7,9,10].

Using the 6 fs pulses, the chirp was varied by inserting thin quartz glass wedges or slabs. It was adjusted (but not measured) in such a way as to obtain the shortest pulses at the location of the autocorrelator. It is likely that the pulses at the input of the Ar cell for supercontinuum generation in Figure 7(*c*) had a slightly negative chirp.

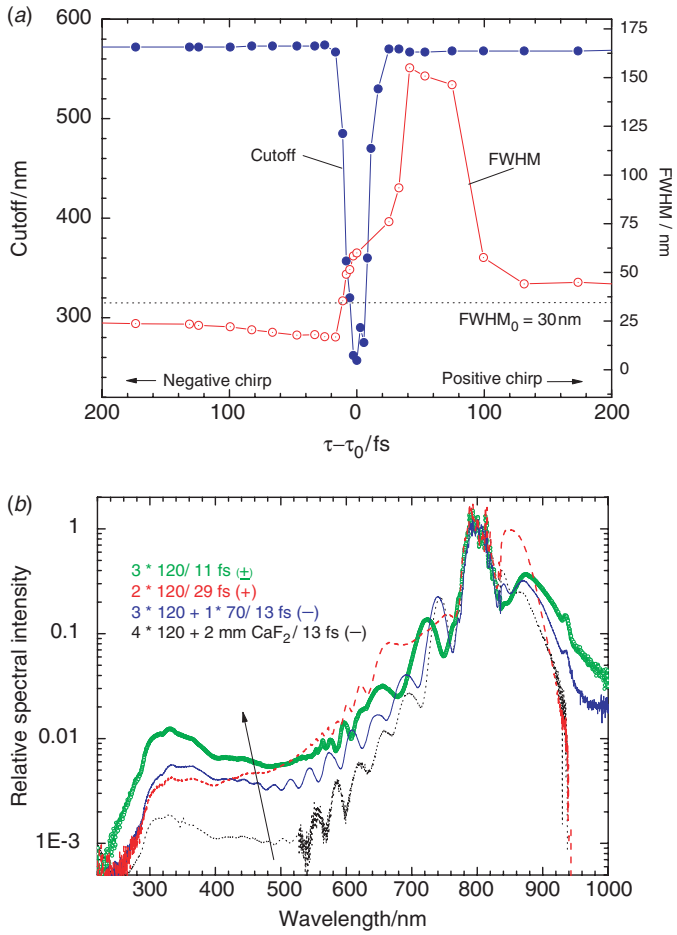

Figure 8. Influence of a chirp of the incident pulses on supercontinuum generation. (*a*) Pulse duration at zero additional chirp $\tau_0 = 45$ fs; the measured lengthening of the pulse duration $\tau - \tau_0$ (which is >0 for both, positive and negative chirp) is indicated instead of the chirp; pulse energy 0.7 mJ, focal length 2 m, argon pressure 1 bar. For conversion to frequency units, multiply the FWHM by 0.469 THz nm^{-1}. The cutoff is the wavelength, where the spectral intensity is 2×10^{-4} of the maximum. (*b*) $\tau_0 = 10$ fs. Meaning of the indicated parameters: e.g. '3*120 + 1*70' stands for three reflections from chirped mirrors of -120 fs^2 and one reflection from a -70 fs^2 mirror; transmission through 2 mm of CaF_2 adds a GDD of 55 fs^2; the resulting pulse duration and sign of the chirp are also indicated. (The color version of this figure is included in the online version of the journal.)

3.7. *Dependence on the Ar partial pressure*

As described in Section 3.1, above a certain optimum energy (0.25–0.35 mJ) of the 10 fs pulses the UV energy dropped again and pointing instabilities and several spots were observed, obviously due to multiple filamentation. Also in the first cell (45 fs pulses) there is such a limit (0.7–1 mJ). Remarkably, the threshold for onset of multiple filamentation in

units of power is nearly the same (16–22 GW) as with the shorter pulses (25–35 GW). Already in [8], we suggested that this limit can be increased by decreasing n_2 by lowering the pressure or partial pressure of Ar. Indeed a mixture of 50% of Ar with He (which has a very small n_2 [16]) at ambient pressure in the first cell (now equipped with two 0.2 mm thick windows of quartz glass; $f = 2$ m) allowed one to use an input energy of 1.3 mJ; after compression by the chirped mirrors we obtained pulses of 9.4 fs and 1 mJ. Using 250 mbar Ar + 700 mbar He with 2 mJ input resulted in 17 fs pulses of 1.5 mJ of energy after compression (loss due to several additional reflections). These stronger pulses were shown in [39] to generate again a supercontinuum extending to 250 nm, and the UV part was used after compression to 30 fs as a widely tunable short-pulse pump source in pump–probe spectroscopy [40] (see also Section 3.8).

Ar–He gas mixtures were also tried in the second cell, which was also equipped with two 0.2 mm thick quartz glass windows, to avoid gas turbulence at open ends with high He partial pressures; the 10 fs pulses ($E_p = 0.3$ mJ) were focused ($f = 1$ m) through it. Figure 9(*a*) shows the output spectra for different mixtures. At low Ar partial pressure one recognizes a weak separate third harmonic (270 nm) besides a supercontinuum of moderate width. For better sensitivity and signal-to-background ratio, it was isolated by reflection with a dielectric mirror and measured by a UV spectrometer (although the broad-band spectrometer also showed traces of it). Increasing the Ar content initially slightly increases the third-harmonic yield, then decreases it again, whereas the supercontinuum steadily broadens and rises, until it covers the third harmonic. Figure 9(*b*) (measured by the UV spectrometer) shows that the third harmonic is not shifted and not broadened: the new maximum at wavelength > 270 nm, growing in and then merging with the 270 nm peak with rising pressure, is obviously the product of the reflection spectrum of the mirror with the spectral edge of the supercontinuum. The broken lines in Figure 9(*b*) indicate how the supercontinuum would probably look without the filter.

3.8. *Pulse duration and compression in the region of 270–320 nm*

It is suggestive to cut out parts of the UV spectrum by means of dielectric mirrors and use this radiation as a source of tunable short pulses. This can be an attractive and simple source for pump radiation in pump–probe experiments, in which also the pulse length can be determined. In [40], we demonstrated this possibility. But since we used a path length of 2.5 m in air, we had to compress the UV pulses again. The compressor consisted of two CaF_2 prisms and a mirror. We obtained 30 fs of pulse duration, which is probably the limit given by third-order dispersion. It can be assumed that the pulses were initially shorter. A vacuum beam path would then avoid pulse lengthening and perhaps the necessity of a compressor.

We therefore prepared the setup of Figure 1(*c*), where the radiation leaving the filament zone (through a 0.6 mm aperture) continues its path only through vacuum (≤ 4 mbar). Indeed in this case the radiation near the cutoff (isolated by 270 nm dielectric mirrors) has a duration of ≤ 10 fs, without the need of any compression, as we reported recently [41]. This promises to be a simple and rugged source for time-resolved spectroscopy, in particular if a practical tuning method is still developed (instead of exchanging dielectric mirrors in the vacuum beam path).

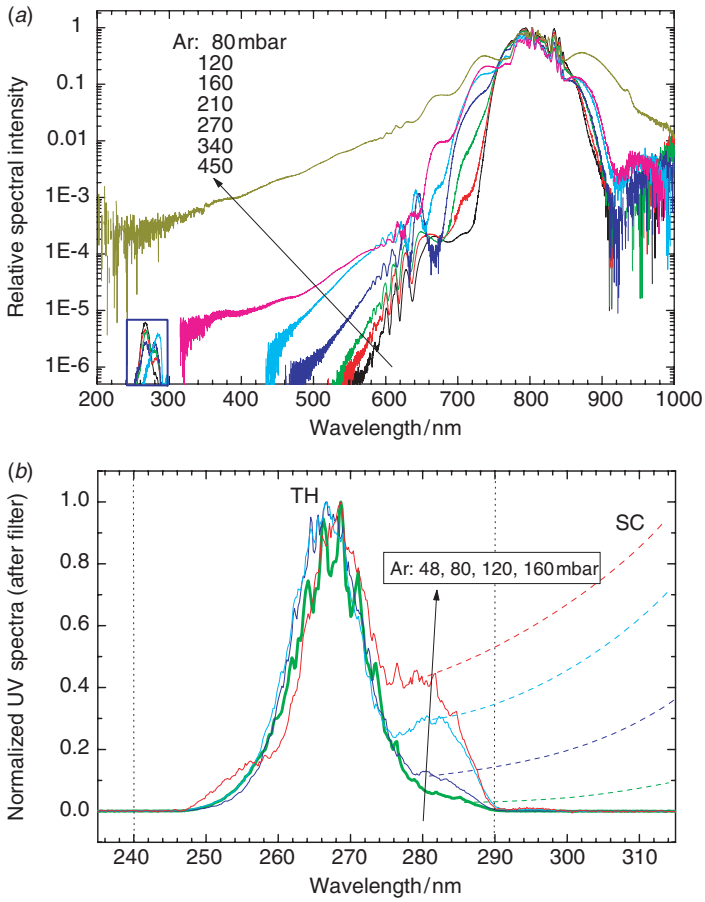

Figure 9. Dependence of the spectra on the Ar partial pressure (difference to 1 bar is He) with pulses of 10 fs and 0.3 mJ. (*a*) Full spectra measured by the broad-band spectrograph, and (in the blue box, up to 270 mbar:) spectra in the region of the third harmonic measured (after reflection at three 270 nm dielectric mirrors) by the (more sensitive) UV spectrometer. (*b*, *c*) Region of the third harmonic (magnification of the blue box in (*a*)); vertical dotted lines indicate the reflection limits (except a side lobe at 296 nm) of the three dielectric mirrors that serve as filters; normalization is to the maxima, so that when the supercontinuum (SC) is growing, the third harmonic (TH) appears reduced. In (*b*) the dashed lines indicate the SC spectra as they would probably be without filtering by the dielectric mirrors. Obviously the 280 nm maximum, growing with pressure, is the product of the SC edge with the filter curve. (*d*) Energies within 240–290 nm measured after the same dielectric mirrors as in (*b*, *c*), with the inset showing a magnification of the lower-pressure part; obviously the nonmonotonic part (maximum at 50–100 mbar) reflects the TH part in (*b*) and the sudden rise above 300 mbar is caused by the SC reaching this spectral region. (The color version of this figure is included in the online version of the journal.)

3.9. *Different gases*

Figure 10(*a*) compares the spectra, generated by the 10 fs pulses ($f = 1$ m) with atmospheric pressure of argon, nitrogen and air. With Ar, the spectrum extends farthest into the UV. It is remarkable that with the three gases the spectra practically coincide in the

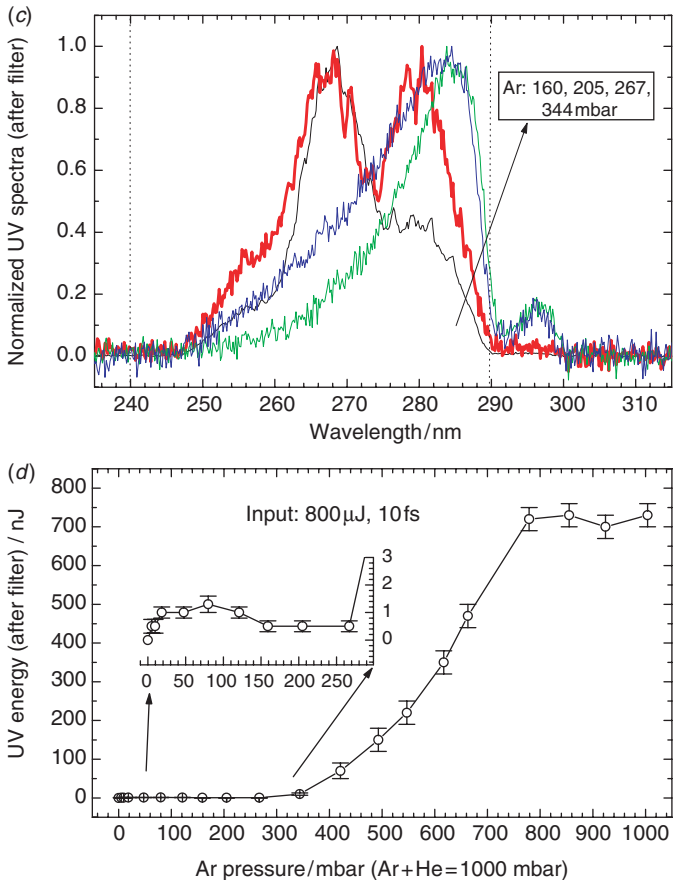

Figure 9. Continued.

central part, down to about 3% of the maximum, although the UV cutoff clearly depends on the gas. The structures visible on the N_2 spectrum can be assigned to the X–B transition in N_2^+ (Section 4.8). A trace of the strongest N_2 peak can also be seen as a small dip in the air spectrum.

Figure 10(*b*) shows a similar comparison for the 45 fs pulses. Obviously the differences between the gases are much greater: with air the cutoff is at 600 nm, although with argon and with the same pulse duration it is easy to reach 250 nm (connected with conical emission, however; see Section 3.2). It was previously reported that supercontinuum spectra in air (with higher powers and longer focal lengths than in Figure 10(*b*)) were limited to about 350 nm [37].

4. Discussion

It is still challenging to understand self-focusing with supercontinuum formation and related phenomena more than qualitatively on a theoretical basis. The common approach

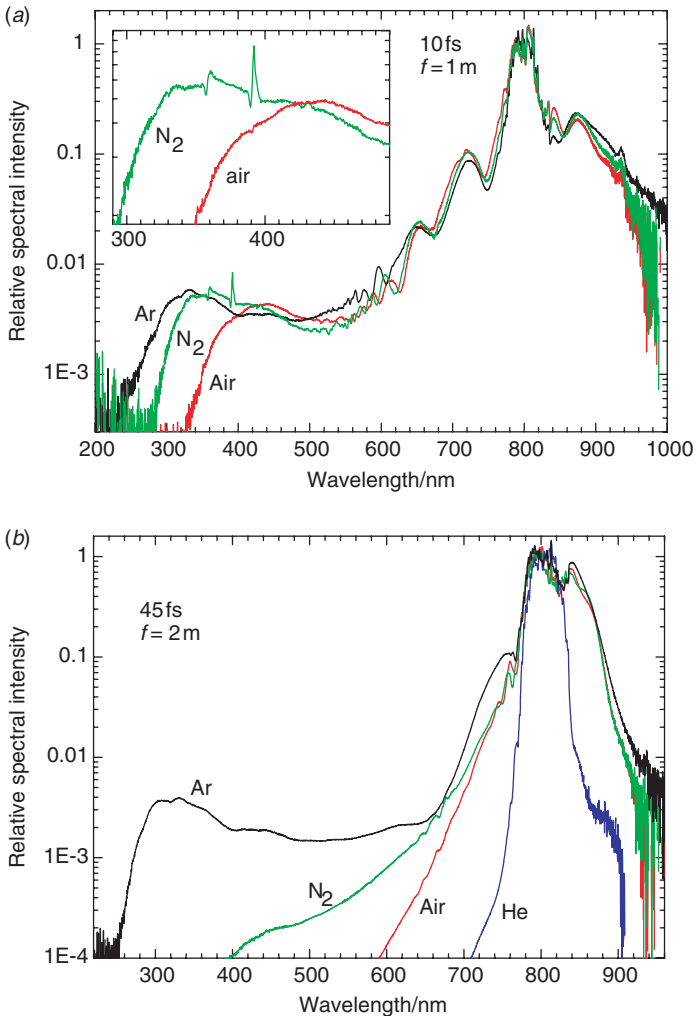

Figure 10. Different gases: (*a*) 10 fs, $f = 1$ m, input pulse energy 0.26 mJ, (*b*) 45 fs, input pulse energy 0.89 mJ, $f = 2$ m. (The color version of this figure is included in the online version of the journal.)

is to calculate the propagation by a nonlinear Schrödinger equation (including the Kerr-effect and plasma contributions to the refractive index). For satisfactory results, an operator for space–time focusing and self-steepening has to be included [15,42]. In this way a semi-quantitative agreement with the UV part of our spectra has been obtained [15]. Such calculations also predict many details such as pulse splitting or compression [15,43,44]. However, already a simplified model description provides insights into the physics and is helpful to check basic assumptions. We present such a model, based on the idea of self-guiding, and use it also for deriving scaling rules in Section 4.1. (For a similar previous model, see below after Equation (8).) In the subsequent sections we discuss the observations in terms of this model and of other qualitative expectations.

4.1. *A model for self-guiding*

It is widely assumed that above a critical power $P_{cr} = \lambda^2/2\pi n_2$ (at which diffraction just compensates Kerr-effect self-focusing), a collapse of the beam is prevented by defocusing by the plasma generated by the high intensities on the axis [1,2,33,45]. The balance between self-focusing and defocusing gives rise to (1) limiting the intensity to a maximum I_{cl} ('clamped intensity'), (2) self-guiding, sometimes over long lengths. The change of the refractive index, Δn, causes a phase shift $\Delta\varphi$ of the wave propagating (with wave number k_0) in z direction:

$$\Delta n = n_2 I - N_e/2N_{cr}, \tag{1}$$

$$\Delta\varphi = \Delta n k_0 z. \tag{2}$$

The first term in (1) represents the Kerr effect, time dependent due to the intensity $I(t)$; for Ar $n_2 = 1.4 \times 10^{-19}\,\mathrm{cm^2\,W^{-1}}$ [46]. The second term is the plasma contribution, with the critical electron density $N_{cr} = \varepsilon_0 m_e \omega^2/e^2$, where e and m_e are the charge and mass of the electron, ω is the laser angular frequency and ε_0 is the dielectric constant of the vacuum; the electron density N_e is usually assumed to be produced by ionizing the gas (density N_g) according to a power law ($m \approx 8$ for Ar at $\lambda = 800\,\mathrm{nm}$):

$$\mathrm{d}N_e/\mathrm{d}t = \sigma^{(m)} I^m N_g \quad \text{or} \quad N_e = \sigma^{(m)} N_g \int_{-\infty}^{t} I^m \,\mathrm{d}t'. \tag{3}$$

The time dependence of the phase shift $\Delta\varphi$ (via the time dependence of I) creates new frequency components, shifted by $\Delta\omega$, because $\Delta\omega = -\mathrm{d}\Delta\varphi/\mathrm{d}t$. It has been shown that the plasma term is usually negligible in its contribution to $\Delta\omega$ [44]. Then one obtains [47] from the derivative of (1):

$$\Delta\omega \propto n_2 I_{cl} \tau_p^{-1} z_{fil}/\lambda. \tag{4}$$

Here we use the filament length z_{fil} for the interaction length at high intensity ($= I_{cl}$). The inverse dependence on the pulse length τ_p results from the derivative of $I(t)$. This equation would predict a symmetric broadening. However, self-steepening (caused by the slower travelling of the pulse maximum as compared with the weaker wings, or caused by the operator mentioned above) after some propagation causes an abrupt slope of the pulse tail, which gives rise to a very large UV shift. This is also the reason why (4) is far from being quantitatively correct. But it is reasonable to assume that $\Delta\omega$ is still a monotonically rising function of the quantities on the right-hand side, in particular of τ_p^{-1} and z_{fil}.

Under conditions of self-focusing, the light is often transmitted ('self-guided') over distances much longer that the diffraction length (Rayleigh length, $2\pi w^2/\lambda$). Self-guiding is here analyzed by comparison with a conventional gradient-index light waveguide. In such a duct with a radial (r) index profile

$$n = n_{ax} + \frac{1}{2} n'' r^2 \quad (n'' = \mathrm{d}^2 n/\mathrm{d}r^2 \text{ at } r = 0;\ n'' < 0) \tag{5}$$

light can be guided with a stable waist w_s if

$$\pi w_s^2 = \lambda/(-n'')^{1/2} \tag{6}$$

(see chapter 16.6 of [48] and Supporting information). This index profile just balances diffraction. Also under conditions of self-focusing a bell-shaped index profile (with n'' to be calculated) can be produced. If a beam can be injected with a Gaussian profile of waist w_s

$$I = I_{ax} \exp\left(\frac{-2r^2}{w_s^2}\right) = \frac{2P(t)}{\pi w_s^2} \exp\left(\frac{-2r^2}{w_s^2}\right), \tag{7}$$

this profile will be stable and hence the index profile will be self-reproduced. Calculating n'' for the Kerr-effect and plasma terms in (1), using (3) and I and I^m from (7), we obtain (see Supporting information)

$$\left(\frac{\pi w_s^2}{2}\right)^{m-1} = m\sigma^{(m)} \frac{N_g}{2N_{cr}} \frac{\int_{-\infty}^{t} P^m \, dt'}{n_2(P - P_{crit})}, \tag{8}$$

where $P_{crit} = \lambda^2/8\pi n_2 = P_{cr}/4$. This is the condition for stable propagation of a beam with waist w_s, which will also lead to a stable index profile. Obviously there is a solution for w_s, if $P > P_{crit}$. But because condition (8) depends on time due to the integral and via $P(t)$, it cannot be expected that it is satisfied at all times. To derive scaling rules, it is suggestive, however, to integrate up to the time, from when the pulse abruptly decays by self-steepening (for single pulses of this shape) and for P the maximum or an average value. Two possible effects of the time dependence of (8) are discussed in Section 4.4 (conical emission) and 4.6 (pulse self-compression).

It is worth noting that for deriving the result (8) we have equated the *curvatures* of Δn_{Kerr} and $|\Delta n_e|$, i.e. $\Delta n''_{Kerr} = -\Delta n''_e$ (+diffraction term), because the curvatures cause the focusing and defocusing. This is in contrast to the widespread (e.g. in [2,3,45]) assumption that the indexes themselves should be equated. On the other hand, with the latter assumption only the factor of m in (8) is lost, a difference which can be absorbed in the parameter $\sigma^{(m)}$. In fact, some scaling rules were derived in Section 1.3.4 and 2.1.2 of [3] on this basis; their pressure and pulse-duration dependences agree with ours (see below).

It is interesting to compare the solution (8) with the results of a *variational method* [35,49,50]. In this method, starting from the nonlinear Schrödinger equation (without self-steepening) a Lagrangian was formed. Assuming for the radiation a trial function that is Gaussian in the radial direction and in time (as above), an equation for the lossless case was derived for the evolution of the waist radius a, that has the form of an equation of motion of a particle in a potential well $U(a)$. This equation has solutions in the form of a waist a periodically oscillating from an initial value a_0 to smaller values, passing through and beyond a minimum of U, and then back to a_0. If one begins with a value for a that corresponds to the minimum of U, this value will not oscillate but remain stationary (a_s). Calculating a_s from the minimum of U results in an equation of the same form as (8) (see Supporting information), so that we can equate $a_s = w_s$. The variational method has

thus found an intuitive interpretation in terms of self-guiding; the other way around, this method predicts that the beam cross-section can oscillate around the stationary value (8). An improved variational solution has been published [50], using as a trial function the sum of two Gaussians. One of them has a narrower waist, representing the plasma-filled region near the axis, whereas the other (with a wider waist) represents the broader background ('reservoir') that is only influenced by diffraction and Kerr-effect focusing. The two partial waves periodically exchange energy. The review [3] discusses also other variational approaches.

It is probably worth checking by the normal propagation equation (as in [15], for example), whether in fact the beam radius would be stable, without oscillating, if at the entrance of the nonlinear medium the beam waist has already a value of w_s ($\approx$160 μm [8]). It may turn out in such a calculation that pulse splitting is avoided in this case, that the filaments become longer and the spectrum broader.

It has also been suggested that the plasma channel has antiguiding properties, which can explain the conical emission of short wavelengths [33] observed with longer pulses (see Section 4.4).

We can use (8) to derive some *scaling rules*, in particular for the common case of $P \gg P_{\mathrm{crit}}$. (For example, one still has single filamentation, if [8] $P \approx 4\ P_{\mathrm{cr}} = 16 P_{\mathrm{crit}}$.)

First we note that at high powers ($P \gg P_{\mathrm{crit}}$) according to (8) the beam cross-section πw_s^2 is proportional to the *power* P, and hence the intensity on the axis is independent of P:

$$\pi w_s^2 \propto P, \tag{9}$$

$$I_{\mathrm{ax}} \propto P^0 \quad \text{or} \quad I_{\mathrm{cl}} \propto P^0. \tag{10}$$

This means that the intensity is clamped. This is experimentally well known [37,38,52]. The proportionality of the beam cross-section πw_s^2 with the laser power or energy (Equation (9)) is exactly reflected in the linear dependence of fluorescence from the plasma found in [52]. The increase of the cross-section of the plasma channel (whose radius should be $= w_s/m^{1/2}$, in agreement with [52]) with the power was observed in [53].

For the dependence on the gas density N_g (*pressure* p), we first note that

$$n_2 \propto p, \tag{11}$$

$$P_{\mathrm{cr}} \propto p^{-1}. \tag{12}$$

The latter equation predicts that for a higher laser power P, one can just take a smaller pressure p to have the same P/P_{cr}, which is consistent with experience (Section 3.7). From (11) we infer that the density dependence cancels on the right-hand side of (8), so that the beam cross-section πw_s^2 and the clamped intensity are pressure independent:

$$I_{\mathrm{cl}} \propto p^0 \quad \text{and} \quad \pi w_s^2 \propto p^0. \tag{13}$$

Recently a p-independent I_{cl} was also derived by the variational method [55]. With the pressure-independent intensity on the axis, Equation (3) implies that the electron density increases with pressure:

$$N_e \propto p. \tag{14}$$

We can also foresee what happens for different *pulse durations*. For a given peak power, the only part of (8) that depends on the pulse length (approximated here by the initial pulse duration τ_i) is the integral. At a time near the end of the pulse, this integral is obviously $\propto \tau_i$, if pulses of the same shape (e.g. Gaussian) are compared. That is, (8) implies

$$\pi w_s^2 \propto \tau_i^{1/(m-1)}, \tag{15}$$

$$I_{ax} = I_{cl} \propto \tau_i^{-1/(m-1)}. \tag{16}$$

Taking a typical value of $m \approx 8$ for the order of ionization, decreasing the pulse duration by a factor of 5 would decrease the beam cross-section by 26% and increase the axial intensity by the same percentage. Taking the electron density N_e from (3) and inserting (16), we find that it increases by the same factor:

$$N_e \propto \tau_i^{-1/(m-1)}. \tag{17}$$

(A factor of $\tau_i^{-m/(m-1)}$ results from I_{ax}^m in (3), and the integral itself contributes another factor of τ_i.) The dependences (16)–(17) agree very well with the pulse-length dependent calculations in [15].

Also *different gases* can be considered. They mainly differ in their nonlinear index of refraction (n_2^*/p) and in their ionization cross-section, $\sigma^{(m)}$. It is their ratio which determines the beam cross-section in (8) and hence the intensity $I_{ax} = I_{cl}$:

$$I_{cl} \propto (n_2^*/\sigma^{(m)})^{1/(m-1)}. \tag{18}$$

$\sigma^{(m)}$ can vary by orders of magnitude, much more than n_2. If the ratio in the parenthesis changed by a factor of 100 on replacing Ar by Ne or He, I_{cl} would increase by a factor of 2; if a higher pressure were chosen to obtain the same n_2 as in Ar of ambient pressure, the (pressure-independent) larger I_{cl} would substantially increase the width of the supercontinuum (more or less according to (4)). On the other hand, at *shorter wavelengths*, the ionization cross-section $\sigma^{(m)}$ is much higher and the order of ionization m is lower. Therefore, a strongly reduced clamped intensity is expected according to (18). This explains why self-focusing of 248 nm radiation is observed to give rise to only a minor spectral broadening [56–58], although harmonics can be observed [59].

In the context of the recently observed negatively chirped radiation from self-focusing [60,61], it is also interesting to consider the prediction of the model for the waveguide dispersion, which is also negative. For a gradient-index guide of radius w_s (as in (5) and (6)), chapter 16.6 of [48] gives the propagation constant k_z as

$$k_z = k_0 - \lambda/\pi w_s^2 = k_0 - (-n'')^{1/2}\lambda/\lambda_0, \tag{19}$$

where k_0 is the wavenumber of propagation without waveguide. Taking the second derivative over ω, using $\lambda_0 = 800$ nm and the experimentally observed [8] $w_s = 160\,\mu$m (Section 3.2), we obtain a group-velocity dispersion of $k_2 = -3.6\,\text{fs}^2\,\text{m}^{-1}$. This is much too small to explain the observed negative chirps (around $-500\,\text{fs}^2$). Hence, they do not arise from waveguide dispersion (see also Section 4.6).

4.2. *The UV cutoff as function of pulse duration, pulse energy and interaction length*

The spectra with pulse duration of 10 fs (e.g. Figures 2 and 3), and even more so those with 6 fs pulses (Figure 7), reach farther into the UV than those reported previously with longer pulses and comparable powers in Ar or air (below the threshold of multiple filamentation). The short wavelengths are generated by (1) the Kerr effect in the decaying part of the pulse, the shift being $\propto \mathrm{d}I/\mathrm{d}t$, and (2) by the plasma over the full length of the pulse, the shift being $\propto I(t)$ [1,2]. Comparing pulses of the same maximum power but different pulse duration τ_p, it seems at first sight that the first term will be $\propto \tau_\mathrm{p}^{-1}$, whereas the second term is independent of τ_p. A closer look reveals that also the plasma term changes to some extent with τ_p: with shorter pulses the clamped intensity and the electron density are slightly higher (Equation (16) and (17)), namely by 26% on decreasing τ_p by a factor of 5. Comparison of the spectra with 45 and 10 fs shows that the effect is much larger. We therefore conclude that the broadening in the UV is mainly due to the Kerr effect in the trailing edge of the pulse. This is a neat confirmation of Gaeta's prediction [42].

This calculation [42] is based on the nonlinear Schrödinger (propagation) equation including self-steepening and terms beyond the slowly-varying-envelope approximation. The steepening arises from the fact that the pulse maximum (where $n_2 I$ is highest) travels more slowly than the rest of the pulse [1,2], a propagation effect not contained in the simple model of Section 4.1. It causes much more broadening than without it. In fact, insertion of numbers into an explicit form [47] of Equation (4) predicts by far too little broadening. This means that the observations also confirm the self-steepening. Using a similar equation, our results (Figures 7 and 5(*b*)) were semiquantitively reproduced in particular in the UV part [15]. Nevertheless, although Equation (4) is not quantitatively correct, we suppose it is good enough to give a quick overlook and predict which parameters will increase the spectral width, even if not proportionally.

The UV cutoff of the 6 fs pulses is much less shifted than expected not only on the basis of a (doubted) proportionality with τ_p^{-1} but also if extrapolated from the pair 45 and 10 fs (Figure 7(*d*)). For interpretation [14] we pointed to the fact that the interaction length at high intensity (i.e. the filament length z_fil) is shorter with the shorter pulses, both in observation [8] and in calculation [15]; in the product $\tau_\mathrm{p}^{-1} z_\mathrm{fil}$ occurring in Equation (4) they partially compensate each other.

At first sight, it seems intuitive that in Figure 3 the UV cutoff is steadily shifted to shorter wavelengths with increasing the pulse energy E_p or power (below the threshold of multiple filamentation). However, one should remember that the clamped intensity is the same in all cases (Equation (10) and context; the power varies in Figure 3 only by a factor of 1.5 and is in all cases well – by a factor of 2.5–4 – above the critical power.) The higher powers only expand the cross-section of the beam (Section 4.1), which in turn will not influence the spectral shift. We suppose that it is z_fil which increases with the power. It is difficult to judge this length by simple inspection, in view of the different powers; and a calculation is not available to our knowledge. But a side observation may support this assumption: E_p has more effect in the UV than in the IR (Figure 3). This is just expected from prolongation of propagation, which develops a steepening of the pulse decay (producing the UV, see above) and a corresponding flattening of the rising edge (producing the IR).

The shift of the UV cutoff with increasing z_{fil} is confirmed by Figure 5(*b*) and by calculation [15]. The fact that this shift deviates from a uniform growth was attributed in [15] to the fact that after some propagation, self-steepening comes to an end and pulse splitting and refocusing set in. Other details such as the development of a spectral maximum around 320 nm (Figure 5(*b*), also Figures 2 and 3) were also reproduced, which gives confidence to the equations used.

Above the limit of multiple filamentation (broken line in Figure 3) the UV yield decreases again. In this case it was clearly visible that the filament at the higher energy was shorter (5–7 cm) than with a single filament (≈12–15 cm) [8]. On the other hand, increasing the power even much more, up to terawatts, has pushed the cutoff to the vacuum UV [16,17,62]. In fact, very long filament lengths were observed thereby, confirming the idea of the influence of z_{fil}. The next section discusses what limits z_{fil}.

4.3. *Termination of the filaments, focal-length dependence, effect of the input diaphragm and pointing stability*

It is not obvious why filamentation should terminate, because self-guiding should result from the balance of the Kerr-effect focusing and defocusing by the plasma. Losses by ionization or conical emission, which can terminate much longer filaments [63], were not measurable with our short filaments [8]. Other suggested mechanisms (moving-focus model [64,65], diffraction by the plasma [66]) are discussed in [15]. It was found there by calculation, that under our conditions the pulses tend to be split after some propagation, so that their power is reduced to near or below the critical power, which can explain the termination [15]. The calculation also reproduced the observed earlier termination with the shorter pulses. Pulse splitting has been observed under conditions of supercontinuum generation (in glass) and attributed to an effect of the dispersion [67]. Pulse splitting induced by normal group-velocity dispersion and filament termination by it was already previously predicted [68–72], and the propagation length needed to cause splitting was estimated in [70]. Although under our conditions the dispersion length $\tau_{\mathrm{p}}^2/(4\ln(2)k'')$ with pulses of $\tau_{\mathrm{p}} = 10$ fs in Ar ($k'' = 20\,\mathrm{fs}^2\,\mathrm{m}^{-1}$) is much longer (1.8 m) than the filaments, the filament termination and pulse splitting also turned out to be sensitive to inclusion of the dispersion term in the calculation [15].

Another support for the mechanism of filament termination by pulse lengthening (splitting) can be inferred from the recent observations of the opposite: pulse self-compression [43,60,61,73], which was observed under similar conditions as ours. (The main difference was the 2–5 times higher pulse energies with the correspondingly smaller Ar pressures. The initial pulse durations were around 50 fs.) The filaments were indeed clearly longer (≥50 cm) than ours, consistent with the idea that they only stop on pulse lengthening. To understand why they then terminate again, one should remember that the shortening was only observed near the axis, whereas the outer spatial wings could even develop some pulse splitting (see in particular [43,73]), which reduces the local power. Perhaps these wings are therefore not refocused and get lost first, so that later on, the central part also becomes too weak to be further self-guided. (The early loss of the spatial wings is not the same as the loss by conical emission, suggested in [62] to cause

filament termination. Conical emission mainly contains the short wavelengths, which are only a small fraction of the total radiation.)

In the presence of many neighboring filaments, an early loss of the outer wing from one filament may feed energy into an adjacent one. If there is not much delay, such a mutual cross-talk can lead to longer self-guiding. In fact, very long self-guiding is observed under conditions of multiple filamentation with correspondingly high powers (e.g. [11–15,65]). The cross-talk is certainly also the reason for the poor pointing stability (introduction to Section 3 and Section 3.1). It could also be the reason of the pulse-to-pulse fluctuation of the spectral shape, observed under such conditions [16,17,62,72].

Whereas the pointing stability is much better with a single filament, experience (also in other experiments, e.g. in [7,9,43,60,61,73,74]) shows that it can be improved even more with a diaphragm before focusing into the Ar cell. This means that the diaphragm may have an additional effect beyond only controlling the energy. Indeed there is an indication that such a perturbation plays a role: if the iris is not carefully centralized on the input beam, the output beam can break up into separate spots whose spectra are different. It has been suggested [75–79] that the near-field diffraction pattern with a maximum on the axis can trigger a filament and thus stabilize it; this effect can even be used to stabilize multiple filaments, if one uses a grid instead of a diaphragm [75–79]. A nonlinear self-stabilization mechanism [80] invokes the gradient of intensity I after the diaphragm, which causes a gradient of the refractive index via $n_2 I$, which focuses the rim of the beam; when the resulting ring approaches the axis, a filament is triggered. According to [81], a circular phase mask can also be used instead of the diaphragm. A phase plate does not cause a loss of energy.

Besides the control of the input energy and the triggering and stabilization of the filaments by spatial modulation, one can expect a third effect of the input iris: reducing its diameter d would (in the absence of nonlinear effects) extend the focal waist by a factor d^{-1} and (in Gaussian optics) the Rayleigh length by a factor of d^{-2}. This would imply a length increase by a factor of 4 on comparing $d = 5\,\text{mm}$ with the initial Gaussian waist (e^{-2}) diameter $2w = 10\,\text{mm}$. On the other hand, in Section 4.2 we concluded that the *filament* length *increases* with d and/or with energy (up to an maximum, reached at $d \approx 5\,\text{mm}$). Obviously the filament length is not predominantly influenced by the Rayleigh length.

Longer focal lengths (or larger f-numbers) lead to longer Rayleigh lengths *and* to longer filaments (see, e.g. [30]). This is mainly known for very high powers, giving rise to multiple filaments, that are investigated for instance for atmospheric monitoring [11–14]. Under conditions of single filamentation with the 45 fs pulses, we also saw a longer filament with focal length $f = 2\,\text{m}$ instead of 1 m (15–20 cm instead of 7–15 cm). This longer z_{fil} probably caused the drastic shift of the UV cutoff in Figure 6(*b*). It would obviously be of practical interest, if the cutoff could be shifted even more, in particular if this method worked also for shorter pulses. However, Figure 6(*a*) shows that with the 10 fs pulses, an increase of f had no effect on the spectrum. It would therefore be desirable to understand the effect of f in order to possibly find a way to prolong z_{fil} or another way to push the UV cutoff further. We are not aware of a theoretical work on the effect of the focal length.

4.4. *Absence of conical emission with the 10 fs pulses*

As in previous reports (see the reviews [1–3]), with the *long* pulses we observed side lobes or rings that contained a larger fraction of short-wavelength radiation than the center (no figure shown). Under some conditions, even an isolated third harmonic was found outside the center. (For example, also in [27], a large part of the third harmonic of 50 fs pulses was found in an outer ring.) To explain such a conical emission, four-wave mixing and other phase-matched mechanisms [1,2] have been invoked. Other models point to an anti-guiding property of the interface between the plasma and the Kerr-effect dominated gas [33] or to diffraction by the plasma [66]. Also a recent high-level theoretical work with longer pulses predicted side lobes of short-wavelength radiation, containing also the largest part of the third harmonic [82]. Conical emission has been considered a characteristic signature of filamentation [83], and conical emission is supposed in Section 4.26 of [3] to be closely connected with supercontinuum generation.

In stark contrast with the longer pulses, conical emission is not noticeable with the 10 fs pulses (Figure 4): the shortest wavelengths are on the axis. This property is reproduced by calculations [14] that include self-steepening and space–time focusing by a term (operator) T; this term goes beyond the slowly-varying-envelope approximation (SVEA) and is more important with shorter pulses. It was introduced by Brabec and Krausz [84]. They said that the inverse of this non-SVEA operator T^{-1} in front of the diffraction term decreases the divergence of the high-frequency components of the spectrum; on the other hand, this operator is not explicitly frequency-dependent. However, the absence of conical emission with the short pulses can be explained by the models invoking anti-guiding or diffraction by the plasma [33,66], if self-steepening is taken into account: these models assume that the refractive index in the plasma is lower than in the surrounding gas, with the difference being more pronounced for shorter wavelengths (due to dispersion), so that in particular the shorter wavelengths are refracted out from the axis [33]. Because the plasma accumulates during the pulse duration, the effect may typically emerge near the end of the pulse, even if (as assumed in our model in Section 4.1) near the pulse maximum the refractive index is still highest on the axis and supports self-guiding at these earlier times. Self-steepening of the trailing edge, which according to the calculations is (due to the T operator) more pronounced for the shorter pulses (Figure 5 in [15]), can give rise to pulses with a shock-like decay from the maximum; in this case no more plasma can accumulate. Hence, with short pulses of this shape the refractive index on the axis will not be sufficiently lowered to values causing anti-guiding and conical emission.

The good collimation is obviously an advantage for application of the short wavelengths, for example in pump–probe spectroscopy [40].

4.5. *Pressure dependence and observation of the third harmonic*

Section 3.7 confirms the prediction in Section 4.1, that one can use higher input powers P and still obtain practically the same spectrum, if the pressure p is reduced by the same factor. In doing so, the ratio P/P_{cr} remains constant (Equation (12)), whereas the electron density N_e changes proportionally to p (Equation (14)). Apparently the former quantity (and hence the Kerr effect) is more important for the (UV) spectrum than N_e. The expectation that the spectrum should only depend on P/P_{cr} ($\propto P \cdot n_2 \propto P \cdot p$) implies

that the dependence on the pressure p (Figure 9(*a*)) should look similar to the dependence on the power P (or energy E, Figure 3). This is in fact qualitatively right. It also implies that the multiple-filamentation limit can also be crossed by raising the pressure instead of the power. Our data of Section 3.7 are all below this limit. For the same reason, one could also expect that the results of [36] at lower power (3.3 GW instead of our 20–30 GW) but higher pressures (7–16 bar of Ar and other gases) would be similar to ours; however, very different phenomena were observed, perhaps due to the much longer pulse durations (150 fs) in [36]. With longer pulses and higher pressures, collisional generation of secondary electrons (optical breakdown) must also be taken into account [85].

With the 10 fs pulses, a weak third harmonic shows up separately from the continuum at low pressures in Figure 9(*a*). With increasing pressure, it does not grow but even slightly decreases, before it is covered by the expanding supercontinuum. Such a nonmonotonic pressure dependence is expected, if phase matching plays a role. In fact, the best yields of harmonics are usually obtained, if they remain in phase with the fundamental. By contrast, the steady expansion and growth of the supercontinuum in Figure 9(*a*) indicates that no phase matching is required for the continuum. It is also worth noting that the third-harmonic maximum is at the expected wavelength (268 nm) in Figure 9, in contrast to the prediction of a long-wavelength shift [86]. The best third-harmonic yield obtained was near 2×10^{-6} ($\approx$1.3 nJ with 800 μJ input, Figure 9(*b*)). A similar efficiency was also reported by Théberge et al. with longer pulses [18]. Much better yields ($1–2 \times 10^{-3}$) can be obtained by focusing through a short cell (length l) filled with Ar ($p^*l \approx 5$ bar mm) with pinholes and He or vacuum outside [40]. This is just the estimated length over which the phases are still matched. Better yields can also be obtained by terminating the filament by a pressure gradient and keeping the subsequent beam path under vacuum, as we have recently demonstrated [41]. This finding is in agreement with the theoretical prediction [25,26] that the third-harmonic yield drops by an order of magnitude within $\approx$1 cm, after the beam leaves the filamentation region; the conversion efficiency then stays constant on further propagation through the gas [25,26]. Obviously the third harmonic is reconverted to the fundamental due to a certain phase mismatch, and this mismatch stays constant thereafter [25,26]. Note also that the termination of the filament by a fine pinhole (instead of the pressure gradient) in Figure 5 does not enhance the third-harmonic yield; it is not detectable in Figure 5(*b*). Because the beam in this case continues propagating through gas, reconversion to the fundamental might also be effective.

Third-harmonic generation has often been found on simple focusing of the fundamental in air or other gases [18,20–30]. The best efficiencies ($1–2 \times 10^{-3}$) were typically observed with short focal lengths [20–24,30], so that there was basically no self-guided filament. Perhaps this is due to the short Rayleigh lengths (over which the nonlinear interaction takes place) in these cases, which were not much longer than the length of phase matching. Tight and loose focusing is compared experimentally in [20,30] and theoretically in [82]. Recently there is interest in the question, whether the third harmonic contributes to the supercontinuum and significantly pushes the UV cutoff to shorter wavelengths, when the two spectral features merge [18,19,25–30,82,87]. Our results indicate that with few-cycle pulses and long filaments this effect is negligible. The theoretical investigation of Kolesik et al. [82] concludes that the two spectral components have a different origin and the supercontinuum generation is not modified by the third harmonic, in agreement with our experimental results.

4.6. *Chirp dependence: connection with self-compression? Are some spectral parts universal?*

Figure 8(*a*) shows that the UV cutoff wavelength is very sensitive to the chirp and (or) the pulse duration τ_p: already an increase from $\tau_p = 45$ fs by 10 fs reduces the spectral broadening by a factor of 2 (cutoff at 420 nm instead of 250 nm). Further increase to $\tau_p \geq 70$ fs suppresses the supercontinuum pedestal totally. This happens in the same way with positive and negative chirp. As said in Section 4.1, the broadening $\Delta\omega$ by the Kerr effect is expected to increase with τ_p^{-1} (even if not proportionally). (The decreased initial intensity I of longer input pulses can be ignored, because I will stabilize in the filament to a value I_{cl}.) The broadening of the pedestal ('cutoff' curve) is obviously more than $\propto \tau^{-1}$ in Figure 8(*a*); the effect would be even clearer, if plotted versus frequency instead of wavelength. Because the short UV wavelengths are generated in the self-steepened trailing edge of the pulse, we suppose that self-steepening is perturbed and eventually suppressed already by a moderate positive or negative chirp. A calculation would be desirable. The cutoff at large chirp in Figure 8(*a*) is identical to that of the spectrum of the incident radiation (see Figure 2). With the 10 fs pulses, where the chirp was varied by using different chirped mirrors and/or inserting a window, the effect seems less dramatic (Figure 8(*b*)). However, for each curve the input iris of the Ar cell was optimized (as in Figure 3) so as to get a maximum output in the UV. Apparently the effect of the chirp on the cutoff can be partially compensated by varying the input energy (iris).

The dependence of the halfwidth (full width at half maximum (FWHM)) in Figure 8(*a*) on the chirp is surprising: with negative chirp a spectral narrowing is observed, but a broadening with zero and in particular with positive chirp. The minimum and maximum FWHM in Figure 8(*a*) (8 and 73 THz) differ by a factor of 9. Usually self-phase modulation (SPM) is aimed at spectral broadening and pulse compression. A pulse lengthening would be obtained instead at the minimum width (8 THz, already at minor chirp), corresponding to a transform-limited pulse duration of 55 fs; this is just the same as the duration of the incident chirped pulse at this minimum ($\tau - \tau_0 = 10$ fs). Note also the more pronounced spectral narrowing of the 6 fs pulses in Figure 7(*c*), corresponding to a lengthening of $\geq$10 fs.

A spectral narrowing of negatively chirped pulses by SPM in quartz glass fibers was observed before [88–90]. Oberthaler and Höpfel [88] recommend the method for the cases, where lengthening is desired; it suffers from less losses than spectral filtering, and Washburn et al. [90] found that in this way a transform-limited pulse of the same duration can be generated from a pulse lengthened to 665 fs (from originally 110 fs) by a negative chirp. The latter result reminds of the finding above (55 fs transform limit resulting from SPM of a 55 fs incident negatively chirped pulse). A gas for SPM would have even less losses than a fiber and permit higher powers. It is worth noting that the initial chirp cannot extend over more than the initial spectral width, whereas SPM can broaden the spectrum, so that it could be expected that the SPM-induced positive chirp can overcompensate a negative initial chirp, in contrast to observation. However, Oberthaler and Höpfel [88] and Planas et al. [89] showed also mathematically that this is not the case even with a very long nonlinear medium. Liu et al. observed a (minor) spectral narrowing of the FWHM, but nevertheless a temporal compression in BK7 glass at $\approx$1000 times the critical power [91]; they ascribed it to spectral reshaping from originally Gaussian to Lorentzian-like form.

Bergé et al. also investigated theoretically the chirp influence on the spatial dynamics of the beam [92].

The observation of spectral narrowing and corresponding pulse stretching of initially negatively chirped pulses is in contrast to experiments, in which pulses were stretched by a negative chirp which is then compensated by normal dispersion in air to shorten the pulses again, so that the filament is triggered in larger distances, for example for lidar [4,11–14,93,94] (see also [4,95]). Hence, this compression occurs before self-focusing, whereas the stretching above must be an effect of the filament.

The strongest broadening of the halfwidth is observed with a positive chirp, which lengthens the incident pulse by a factor of 2 ($\tau - \tau_0 = 40$–70 fs in Figure 8(*a*)). This seems to us not understandable in the standard model. However, there may be a connection with other recent observations: in experiments similar to ours but with energies higher by a factor of 2.5–5, self-compression and negative chirps were found after self-focusing in argon [43,60,73]. The negative chirp induced by the filament perhaps compensates a positive chirp of a (long) input pulse and shortens it thereby, so that SPM is stronger than with a transform-limited incident pulse. (It could also compensate the normal dispersion on further propagation and thus cause the self-compression in the experiments of [43,60,73]). Hence, we suggest that the FWHM maximum at positive chirp in Figure 8(*a*) has the same origin as the negative chirps and self-compression observed [43,60,73] at higher pulse energies. These phenomena have been interpreted [43] by the moving-focus model: an early slice of the pulse sees only little plasma on focusing to the axis, whereas a later slice sees more, so that it can partially catch up the earlier one due to the refractive index lowered by the plasma. The interpretation thus invokes the lowering of the refractive index by the electrons, whose magnitude increases with time with the plasma density [73].

Strickland and Corkum [72] observed that the broadening of the spectra around the pump wavelength is universal, being insensitive to the duration and power of the input pulse and to the nonlinear medium. In fact, the halfwidths (and 10%-widths) of our spectra are also very similar, comparing different input powers (Figure 3), pulse durations (Figure 7(*d*)), focal lengths (Figure 6(*b*)) and different gases (Figure 10). This width would correspond in the transform limit to a pulse duration around 10 fs, as in [72]. On the other hand, the initial chirp can cause a drastic change (by a factor of 9 in Figure 8(*a*)) of the halfwidth. Because the initial chirp is usually not measured but simply optimized (for best UV yield in our experiment), we suppose that the 'universality' of the halfwidth is to some extent accidental.

4.7. *Compression and pulse duration in the UV and application for pump–probe spectroscopy*

In Section 4.2 we found evidence for the prediction [42] that the UV radiation is mainly or only generated by the Kerr effect in the abrupt drop of the intensity in the trailing edge, caused by self-steepening of the pulse. The UV pulse can therefore be expected to be not longer than this optical shock. According to the calculations [15], after 5 cm of propagation in the filament the intensity on the axis drops from 90% to 10% within 3 to 1 fs, starting with initial pulses of 10 and 6 fs, respectively. However, on further propagation the pulses lengthen again and can split [15]. It seems therefore attractive to

stop the filament after about 5 cm by a pressure drop at an aperture, beyond which the argon is pumped away. Indeed we obtained 10 fs UV pulses from incident pulses of the same duration in such a setup (Section 3.8 and [41]). This is longer than predicted; however, the calculation was only local (not integrated over the cross-section). But the observation confirms that the conversion to the supercontinuum can take place within the original pulse duration and that lengthening by pulse splitting is avoided by terminating the filament by a pressure gradient.

In the setup without pressure gradient (Figure 1(*b*)), after generation in the filament, the UV pulses pass through additional argon, through air (≈2.5 m) and optical elements, which lengthen the pulses by dispersion. To compensate for it, we used a prism compressor in [40] (which is also used for tuning) and obtained a duration of 30 fs at wavelengths in the range 270 to 320 nm. By comparison with the third harmonic, generated in a much shorter Ar cell but with the same optical path otherwise, we concluded that this duration is limited by higher-order dispersion that is not compensated. A vacuum beam path avoids such effects, as mentioned above.

Such a source of tunable short (30 or 10 fs) UV pulses is particularly attractive for pump–probe spectroscopy. The gas supercontinuum provides enough energy even for use as a (tunable) *pump*, and we demonstrated this possibility already with two examples [41,96]. Competing high-power methods are all challenging in alignment and operation, as pointed out in [40]. The limit of energy (≤0.25 mJ at 1 bar of Ar, or more at lower pressure) in the filament method is much higher than would be possible in supercontinuum generation in condensed matter. The latter method has long provided the *probe* radiation for broad-band transient absorption spectroscopy (see, e.g. [97]). In this case, 10–20 μJ are focused into a disk of CaF_2, quartz glass, sapphire or D_2O. The generated spectrum is more or less limited to about 350 nm (see, e.g. [37,40]), although a weak tail seems to suffice for transient absorption down to 260 nm (e.g. [98]). Probably with the solid material there is multiple filamentation, causing spectral pulse-to-pulse fluctuation. Furthermore, dispersion gives rise to a delay of the different wavelengths versus each other by hundreds of femtoseconds, which requires a correction in transient absorption spectroscopy [97]. No delay greater than the pulse length (10 fs) is expected in our case, if dispersive material is avoided after the generation of the supercontinuum.

4.8. *Self-focusing in nitrogen and air*

Replacing argon by nitrogen or air shifts the UV cutoff to slightly or moderately longer wavelengths, respectively, in the case of 10 fs pulses (Figure 10(*a*)). With the 45 fs pulses, the effect is much more pronounced (Figure 10(*b*)). Nitrogen and argon are very similar in their nonlinear index n_2 [45] and their ionization probability $\sigma^{(m)}$ [99], so that Equation (8) would not predict much difference. In air, however, the electrons are produced by ionization of oxygen, whose $\sigma^{(m)}$ is higher by a factor of 10^3–10^2 for 30–50 TW cm^{-2} than that of N_2 and Ar [99] due to its smaller ionization energy (12.5 eV versus 15.6 and 15.75 of N_2 and Ar). (According to Schröder [100], electrons from ionization of H_2O in ambient air are also not negligible.) The higher electron density reduces I_{cl} (Section 4.1). Equation (18) would predict a reduction by a factor of ≥2 (taking into account the oxygen partial pressure), implying a corresponding decrease of the broadening (Equation (4)).

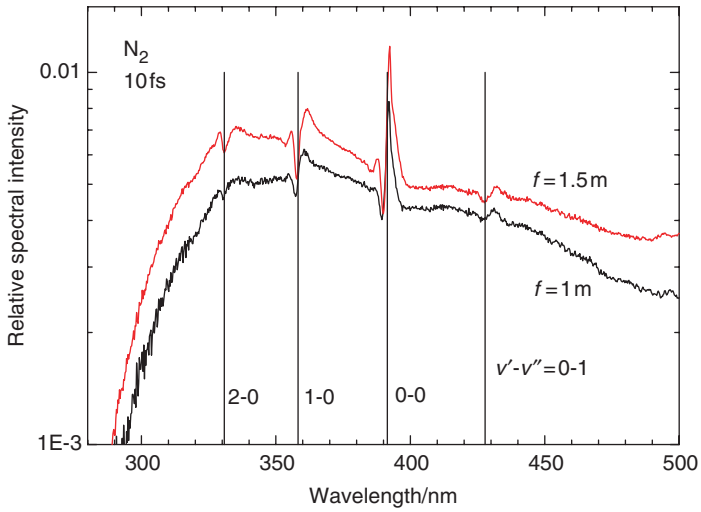

Figure 11. N_2 structures (details), using the 10 fs pulses and focal lengths of $f = 1$ and 1.5 m and input pulse energies of 0.26 and 0.38 mJ. The wavelengths for the different vibrational transitions (with quantum numbers for the upper and lower states, v' and v'', respectively) are from [101]. (The color version of this figure is included in the online version of the journal.)

Compared with this expectation, the effect is obviously smaller in the case of the 10 fs pulses, but larger with the longer pulses. On the other hand, the equations in Section 4.1 are only valid for a given filament length, and this length might be different for the two gases and can depend on the pulse duration.

One can ask why the effect is absent in the halfwidth: the visible and near-IR spectral parts with all three gases are nearly identical. However, the parameters (input iris and initial chirp) in all measurements have been varied for best UV output. The example with the chirp (Section 4.6) shows that such parameters may not act in the same sense for the UV cutoff and the halfwidth.

The conspicuous structures in the spectrum with nitrogen practically coincide with the vibrational structure in the $X\,^2\Sigma_g^+ \leftrightarrow B\,^2\Sigma_u^+$ band of N_2^+ (see e.g. [101,102]). This is shown in detail in Figure 11. Obviously several features are superimposed in the individual bands.

(1) All bands contain a dispersion-shaped feature, as is normally observed for the wavelength dependence of the refractive index around an absorption band. This shape is most clearly recognized in the longest-wavelength (1–0) band.
(2) An absorption, appearing as downward peaks in the 0–0, 0–1 and 0–2 transitions.
(3) A stimulated emission (amplified spontaneous emission), appearing as a prominent upward peak in the 0–0 transition, possibly also superimposed on the other features in the 0–1 transition.

Probably minor shifts versus the wavelengths of the literature [101] can be largely explained as an effect of this superposition. In fact, the wavelengths of the 0–0 absorption peaks seem to depend (with shifts ≤ 1 nm) on the strength of the adjacent emission peak (compare the spectra at $f = 1$ and 1.5 m and of air). Note that absorption and emission

peaks are not expected to coincide exactly, since the gain is usually higher on the P-branch lines, which are at longer wavelengths than the origin.

Stimulated emission in this band of N_2^+ has already previously been observed by the Chin group from back-scattering from a filament in air [103]. The authors suggested that the X (ground) and B (excited) states of N_2^+ are both produced by the high-field laser ionization, with comparable efficiency but initially without inversion. Then recombination of the electrons would be faster with the ground state than with the excited state of N_2^+, thus depleting the former and creating an inversion between the B and X levels. Our observations confirm this mechanism: for absorption, the lower levels must be more populated than the upper ones, and the other way around for stimulated emission. Because absorption (negative peaks) and emission (positive peaks) are observed in the same transitions of the (time-integrated) spectrum, there must be a time delay, with the population inversion developing only later. According to [103], recombination populates the C state of neutral N_2, which then in [103] showed stimulated emission in the $0 \rightarrow 1$ band to the B state at 357 nm. We did not observe this emission (or any other in this band), which would overlap with that of the 1–0 transition (358 nm) of the N_2^+ bands.

The B $^2\Sigma_u^+$ state of N_2^+ corresponds to a hole in the HOMO-2 orbital of N_2. It was suggested that an electron is eliminated from this orbital in the same way, and apparently with not much less efficiency, as from the HOMO by direct field ionization [103]. Field ionization should be a vertical process. If population of a real intermediate state in the neutral or ion plays a role, the ionization will not necessarily fully preserve the interatomic distance. For a vertical process, one expects that the $v' = 1$ level in the B state of the ion has a population n_1 of 8% relative to the $v' = 0$ level, as to conclude from the photoelectron spectrum [104]. However, the intensity ratios of the dispersion features at the $1 \rightarrow 0$ and $0 \rightarrow 1$ transitions (whose Franck–Condon factors differ only little, see Table 94 in [102]) is 0.3, indicating $n_1 / n_0 \approx 0.3$, clearly larger than 0.08. Apparently, reaching the B state of N_2^+ is favored by population of a real intermediate state, that has a larger NN distance and therefore supports population of higher vibrational levels. This is also suggested by the high B-state population (which is comparable to that of the X state, see above), which would not be expected with pure field ionization in view of the large energy difference leading to the two ion states (18.75 versus 15.6 eV [104]).

The dispersion-like features in the N_2 supercontinuum deserve additional comments. Such structures do not appear in the spectra of absorbing trace gases in air, for whose remote detection the supercontinuum can be used (see e.g. [11]). In contrast to the trace gases, the time-dependent concentration of N_2^+ provides a time-dependent refractive index in addition to the plasma term $\Delta n_{\mathrm{plasma}} (= N_e / N_{cr}$ in Equation (1)), which in turn contributes to self-phase modulation. It is higher on the long-wavelength side of the resonance (as observed), if the lower state (X) is more populated than the upper one (B); this confirms once more that an inversion and emission develop only after a time delay. The exact mathematics of such a dispersive contribution to the supercontinuum is not straightforward, however, because the index of refraction near the resonance depends on time *and* on frequency. In principle, the observation of the N_2^+ structures could serve for determination of the density of N_2^+ and hence of the electrons on the axis, because the transition probabilities are known [105,106]. In this case, the transmitted radiation should be limited to the axis by means of an aperture.

5. Conclusion

A number of features of the supercontinuum produced by self-focusing of few-cycle pulses (duration 10 fs or shorter) in Ar, that differ from the case of longer pulses, seems promising for applications. The most prominent is the *very broad spectral pedestal*, which is interesting for spectroscopic applications, in particular for pump–probe spectroscopy. It is most attractive to start with 10 fs pulses, which can be simply made by self-phase modulation in argon and chirped-mirror compression. In this case, the supercontinuum extends in the UV down to 250 nm (and even to 210 nm with 6 fs pulses). A remarkable advantage is that with these pulses all the spectrum, including the shortest wavelengths, is collimated and shows *no conical emission*. This property may also be attractive, if further amplification and pulse shortening is desired. Limiting the input energy by an iris, so that only a single filament is generated, provides a source of tunable radiation with rather good *pulse-to-pulse stability* of the spectrum, the resulting energies, peak powers, pulse shapes and the beam direction. Previously, comparably short wavelengths have also been reached with longer pulses, but only at much higher powers; the radiation therefore suffered from multiple filamentation and the corresponding instabilities and from conical emission.

In contrast to spectral broadening in condensed matter, the gas supercontinuum provides enough energy also for use as a (tunable) pump in transient spectroscopy. This has already been demonstrated [40,41,96]. Recent results show that the supercontinuum pulses are *intrinsically short*, remaining as short as the fundamental, if after their generation one avoids dispersive material (Section 4.7) [41]. It was argued [40] that other methods, providing short durations of tunable UV light, are much more challenging in alignment and operation.

To extend the range of possibilities of the supercontinuum, it is helpful to understand its *mechanism*. Numerical calculations have contributed much in this sense and have been valuable by their predictions; there is still much progress in this field. But simple qualitative models are also justified, in particular if they can provide scaling rules or predict trends. In Section 4.1 we present such a *model, based on self-guiding* by a balance between focusing by the Kerr effect and defocusing by diffraction and by the plasma. It can also be derived by a variational method. In agreement (though not quantitative) with the experiment, it predicts the dependence of broadening on pulse duration, interaction length, pressure or ionization probability of the gas, for example, and provides some intuitive interpretations.

For even further improvement of the supercontinuum source, a better understanding seems to us still desirable in several respects.

- The termination of the filaments. According to numerical calculation (see Section 4.3), it is caused by pulse splitting, which lowers the power to below P_{cr}. It seems that even a small dispersion such as in Ar can cause such a splitting. An intuitive model or some scaling rules would be desirable.
- The influence of the focal length: why does it have a drastic effect on the filament length z_{fil} and spectral width with 45 fs pulses but not in the case of 10 fs pulses? Is there any influence of a hidden parameter? Is there any other simple method to increase z_{fil} and thus push the cutoff further into the UV?

- A remarkable observation, that is very welcome in applications, is the absence of conical emission with 10 fs pulses. It seems to us worth some further theoretical considerations, although we presented a qualitative interpretation in Section 4.4.
- The unusual chirp dependence: the UV cutoff is very sensitive to the initial chirp, more than expected on the basis of the chirp-induced pulse stretching; but this sensitivity can in part be compensated by variation of the input iris or energy (with the 10 fs pulses). Surprisingly the halfwidth (at least with the 45 fs pulses) is increased by a large factor, if the initial chirp is positive (although this lengthens the initial pulse by a factor ≥ 2). In Section 4.6 we discussed whether this observation is perhaps connected with observed negative chirps and pulse compression at higher energies.

It has already been demonstrated how useful is the supercontinuum, generated in Ar with 10 fs pulses, as a simple and rugged source of tunable ultrashort pulses as a pump in transient spectroscopy [40,41,96] (see also Section 4.7). It would certainly be even more attractive to extend the spectral range further to shorter wavelengths. This can either be done by starting with shorter pulses (see Figure 7) or by extending the filament length. In particular for the latter objective, a better theoretical understanding is desirable, as discussed above.

Acknowledgements

This work was supported by the Deutsche Forschungsgemeinschaft (project FU 363/1) and the European Union's Human Potential Program under contract MRTN-CT-2003-505138 (XTRA). We thank S. Panja for his contribution to the first measurements (see [8]). We also appreciate the cooperation with A. Baltuška, E. Goulielmakis, F. Krausz and M. Uiberacker in the experiments with their 6 fs laser (see [15]).

Note

1. In cooperation with Thomas Otto et al. Fraunhofer-Institut für Zuverlässigkeit und Mikrointegration, Chemnitz.

References

[1] Alfano, R.R. *The Supercontinuum Laser Source;* Springer: New York, 1989.
[2] Chin, S.L.; Hosseini, S.A.; Liu, W.; Luo, Q.; Théberge, F.; Aközbek, N.; Becker, A.; Kandidov, V.P.; Kosareva, O.G.; Schroeder, H. *Can. J. Phys.* **2005,** *83,* 863–905.
[3] Couairon, A.; Mysyrowicz, A. *Phys. Rep.* **2007,** *441,* 47–189.
[4] Bergé, L.; Skupin, S.; Nuter, R.; Kasparian, J.; Wolf, J.P. *Rep. Progr. Phys.* **2007,** *70,* 1633–1713.
[5] Brabec, T.; Krausz, F. *Rev. Mod. Phys.* **2000,** *72,* 545–591.
[6] Nisoli, M.; De Silvestri, S.; Svelto, O. *Appl. Phys. Lett.* **1996,** *68,* 2793–2795.
[7] Hauri, C.P.; Kornelis, W.; Helbing, F.W.; Heinrich, A.; Couairon, A.; Mysyrowicz, A.; Biegert, J.; Keller, U. *Appl. Phys. B* **2004,** *79,* 673–677.
[8] Trushin, S.A.; Panja, S.; Kosma, K.; Schmid, W.E.; Fuß, W. *Appl. Phys. B* **2005,** *80,* 399–403.
[9] Hauri, C.P.; Guandalini, A.; Eckle, P.; Kornelis, W.; Biegert, J.; Keller, U. *Opt. Express* **2005,** *13,* 7541–7547.

[10] Guandalini, A.; Eckle, P.; Anscombe, M.; Schlup, P.; Biegert, J.; Keller, U. *J. Phys. B* **2006,** *39,* S257–S264.
[11] Chen, X.; Li, X.; Liu, J.; Wei, P.; Ge, X.; Li, R.; Xu, Z. *Opt. Lett.* **2007**, *32*, 2402–2404.
[12] Rairoux, P.; Schillinger, H.; Niedermeier, S.; Rodriguez, M.; Ronneberger, F.; Sauerbrey, R.; Stein, B.; Waite, D.; Wedekind, C.; Wille, H.; et al. *Appl. Phys. B* **2000,** *71,* 573–580.
[13] Méjean, G.; Kasparian, J.; Salmon, E.; Yu, J.; Wolf, J.P.; Bourayou, R.; Sauerbrey, R.; Rodriguez, R.; Wöste, L.; Lehmann, H.; et al. *Appl. Phys. B* **2003,** *77,* 357–359.
[14] Méchain, G.; Couairon, A.; André, Y.B.; D'Amico, C.; Franco, M.; Prade, B.; Tzortzakis, S.; Mysyrowicz, A.; Sauerbrey, R. *Appl. Phys. B* **2004,** *79,* 379–382.
[15] Aközbek, N.; Trushin, S.A.; Baltuška, A.; Fuß, W.; Goulielmakis, E.; Kosma, K.; Krausz, F.; Panja, S.; Uiberacker, M.; Schmid, W.E.; et al. *New J. Phys.* **2006,** *8,* 177-1–12.
[16] Nishioka, H.; Odajima, W.; Ueda, K.; Takuma, H. *Opt. Lett.* **1995,** *20,* 2505–2507.
[17] Nishioka, H.; Ueda, K. *Appl. Phys. B* **2003,** *77,* 171–175.
[18] Théberge, F.; Liu, W.; Luo, Q.; Chin, S.L. *Appl. Phys. B* **2005,** *80,* 221–225.
[19] Bergé, L.; Skupin, S.; Méjean, G.; Kasparian, J.; Yu, J.; Frey, S.; Salmon, E.; Wolf, J.P. *Phys. Rev. E* **2005,** *71,* 016602-1–13.
[20] Backus, S.; Peatross, J.; Zeek, Z.; Rundquist, A.; Murnane, M.; Kapteyn, H.C. *Opt. Lett.* **1996,** *21,* 665–667.
[21] Peatross, J.; Backus, S.; Zhou, J.; Murnane, M.M.; Kapteyn, H.C. *J. Opt. Soc. Am. B* **1998,** *15,* 186–192.
[22] Fedotov, A.B.; Koroteev, N.I.; Loy, M.M.T.; Xiao, X.; Zheltikov, A.M. *Opt. Commun.* **1997,** *133,* 587–595.
[23] Siders, C.W.; Turner, N.C. III; Downer, M.C.; Babine, A.; Stepanov, A.; Sergeev, A.M. *J. Opt. Soc. Am. B* **1996,** *13,* 330–335.
[24] Marcus, G.; Ziegler, A.; Henis, Z. *J. Opt. Soc. Am. B* **1999,** *16,* 792–800.
[25] Aközbek, N.; Iwasaki, A.; Becker, A.; Scalora, M.; Chin, S.L.; Bowden, C.M. *Phys. Rev. Lett.* **2002,** *89,* 143901-1–4.
[26] Aközbek, N.; Becker, A.; Scalora, M.; Chin, S.L.; Bowden, C.M. *Appl. Phys. B* **2003,** *77,* 177–183.
[27] Théberge, F.; Aközbek, N.; Liu, W.; Gravel, J.F.; Chin, S.L. *Opt. Commun.* **2005,** *245,* 399–405.
[28] Théberge, F.; Luo, Q.; Liu, W.; Hosseini, S.A.; Sharifi, S.M.; Chin, S.L. *Appl. Phys. Lett.* **2005,** *87,* 081108-1–3.
[29] Alexeev, I.; Ting, A.C.; Gordon, D.F.; Briscoe, E.; Hafizi, B.; Sprangle, P. *Opt. Lett.* **2005,** *30,* 1503–1505.
[30] Yang, H.; Zhang, J.; Zhao, L.Z.; Li, Y.J.; Teng, H.; Li, Y.T.; Wang, Z.H.; Chen, Z.L.; Wei, Z.Y.; Ma, J.X.; et al. *Phys. Rev. E* **2003,** *67,* 015401(R)-1–4.
[31] Kienberger, R.; Hentschel, M.; Spielmann, C.; Reider, G.A.; Milosevic, N.; Heinzmann, U.; Drescher, M.; Krausz, F. *Appl. Phys. B* **2002,** *74,* S3–S9.
[32] Corkum, P.B.; Rolland, C. In *The Supercontinuum Laser Source*; Alfano, R.R., Ed.; Springer: New York, 1989; pp. 318–336.
[33] Nibbering, E.T.J.; Curley, P.F.; Grillon, G.; Prade, B.S.; Franco, M.A.; Salin, F.; Mysyrowicz, A. *Opt. Lett.* **1996,** *21,* 62–64.
[34] Chin, S.L.; Aközbek, N.; Proulx, A.; Petit, S.; Bowden, C.M. *Opt. Commun.* **2001,** *188,* 181–186.
[35] Aközbek, N.; Bowden, C.M.; Chin, S.L. *J. Mod. Opt.* **2002,** *49,* 475–486.
[36] Koprinkov, I.G.; Suda, A.; Nurhuda, M.; Wang, P.; Midorikawa, K. *Phys. Rev. A* **2006,** *74,* 053819-1–11.
[37] Liu, W.; Petit, S.; Becker, A.; Aközbek, N.; Bowden, C.M.; Chin, S.L. *Opt. Commun.* **2002,** *202,* 189–197.

[38] Kasparian, J.; Sauerbrey, R.; Chin, S.L. *Appl. Phys. B* **2000,** *71,* 877–879.
[39] Becker, A.; Aközbek, N.; Vijayalakshmi, K.; Oral, E.; Bowden, C.M.; Chin, S.L. *Appl. Phys. B* **2001,** *73,* 287–290.
[40] Trushin, S.A.; Fuß, W.; Kosma, K.; Schmid, W.E. *Appl. Phys. B* **2006,** *85,* 1–5.
[41] Trushin, S.A.; Kosma, K.; Fuß, W.; Schmid, W.E. *Opt. Lett.* **2007,** *32,* 2432–2434.
[42] Gaeta, A.L. *Phys. Rev. Lett.* **2000,** *84,* 3582–3585.
[43] Couairon, A.; Biegert, J.; Hauri, C.P.; Kornelis, W.; Helbing, F.W.; Keller, U.; Mysyrowicz, A. *J. Mod. Opt.* **2006,** *53,* 75–85.
[44] Couairon, A.; Franco, M.; Mysyrowicz, A.; Biegert, J.; Keller, U. *Opt. Lett.* **2005,** *30,* 2657–2659.
[45] Braun, A.; Korn, G.; Liu, X.; Du, D.; Squier, J.; Mourou, G. *Opt. Lett.* **1995,** *20,* 73–75.
[46] Nibbering, E.T.J.; Grillon, G.; Francois, M.A.; Prade, B.S.; Mysyrowicz, A. *J. Opt. Soc. Am. B* **1997,** *14,* 650–660.
[47] Manassah, J.T. In *The Supercontinuum Laser Source*; Alfano, R.R., Ed.; Springer: New York, 1989; pp. 184–294.
[48] Siegman, A.E. *Lasers;* University Science Books: Mill Valley: CA, 1986.
[49] Aközbek, N.; Bowden, C.M.; Talebpour, A.; Chin, S.L. *Phys. Rev. E* **2000,** *61,* 4540–4549.
[50] Yu, W.; Yu, M.Y.; Zhang, J.; Qian, L.J.; Yuan, X.; Lu, P.X.; Li, R.X.; Sheng, Z.M.; Liu, J.R.; Xu, Z.Z. *Phys. Plasmas* **2004,** *11,* 5360–5363.
[51] Arévalo, E.; Becker, A. *Phys. Rev. E* **2005,** *72,* 026605-1–8.
[52] Becker, A.; Aközbek, N.; Vijayalakshmi, K.; Oral, E.; Bowden, C.M.; Chin, S.L. *Appl. Phys. B* **2001,** *73,* 287–290.
[53] Liu, W.; Théberge, F.; Arevalo, E.; Gravel, J.F.; Becker, A.; Chin, S.L. *Opt. Lett.* **2005,** *30,* 2602–2604.
[54] Deng, Y.P.; Zhu, J.P.; Ji, Z.G.; Liu, J.S.; Shuai, B.; Li, R.X.; Xu, Z.Z.; Théberge, F.; Chin, S.L. *Opt. Lett.* **2006,** *31,* 546–54.
[55] Arévalo, E. *Phys. Rev. E* **2006,** *74,* 016602-1–5.
[56] Schwarz, J.; Rambo, P.; Diels, J.C.; Kolesik, M.; Wright, E.M.; Moloney, J.V. *Opt. Commun.* **2000,** *180,* 383–390.
[57] Tzortzakis, S.; Lamouroux, B.; Chiron, A.; Franco, M.; Prade, B.; Mysyrowicz, A.; Moustaizis, S.D. *Opt. Lett.* **2000,** *25,* 1270–1272.
[58] Tzortzakis, S.; Lamouroux, B.; Chiron, A.; Moustaizis, S.D.; Anglos, D.; Franco, M.; Prade, B.; Mysyrowicz, A. *Opt. Commun.* **2001,** *197,* 131–143.
[59] Kortsalioudakis, N.; Tatarakis, M.; Vakakis, N.; Moustaizis, S.D.; Franco, M.; Prade, B.; Mysyrowicz, A.; Papadogiannis, N.A.; Couairon, A.; Tzortzakis, S. *Appl. Phys. B* **2005,** *80,* 211–214.
[60] Stibenz, G.; Zhavoronkov, N.; Steinmeyer, G. *Opt. Lett.* **2006,** *31,* 274–276.
[61] Hauri, C.P.; Trisorio, A.; Merano, M.; Rey, G.; Lopez-Martens, R.B.; Mourou, G. *Appl. Phys. Lett.* **2006,** *89,* 151125-1–3.
[62] Nishioka, H.; Ueda, K. *SPIE Proc.* **1998,** *3734,* 10–14.
[63] Couairon, A. *Appl. Phys. B* **2003,** *76,* 789–792.
[64] Brodeur, A.; Chien, C.Y.; Ilkov, F.A.; Chin, S.L.; Kosareva, O.G.; Kandidov, V.P. *Opt. Lett.* **1997,** *22,* 304–306.
[65] Lange, H.R.; Grillon, G.; Ripoche, J.F.; Franco, M.A.; Lamouroux, B.; Prade, B.S.; Mysyrowicz, A.; Nibbering, E.T.J.; Chiron, A. *Opt. Lett.* **1998,** *23,* 120–122.
[66] Liu, W.; Luo, Q.; Théberge, F.; Xu, H.L.; Hosseini, S.A.; Sarifi, S.M.; Chin, S.L. *Appl. Phys. B* **2006,** *82,* 373–376.
[67] Ranka, J.K.; Schirmer, R.W.; Gaeta, A.L. *Phys. Rev. Lett.* **1996,** *77,* 3783–3786.
[68] Rothenberg, J.E. *Opt. Lett.* **1992,** *17,* 583–585.
[69] Chernev, P.; Petrov, V. *Opt. Lett.* **1992,** *17,* 172–174.

[70] Henz, S.; Herrmann, J. *Phys. Rev. A* **1999,** *59,* 2528–2531.
[71] Kandidov, V.P.; Golubtsov, I.S.; Kosareva, O.G. *Quantum Electron.* **2004,** *34,* 348–354.
[72] Strickland, D.; Corkum, P.B. *J. Opt. Soc. Am. B* **1994,** *11,* 492–497.
[73] Skupin, S.; Stibenz, G.; Bergé, L.; Lederer, F.; Sokollik, T.; Schnürer, M.; Zhavoronkov, N.; Steinmeyer, G. *Phys. Rev. E* **2006,** *74,* 056604–056601-056609.
[74] Park, J.; Imran, T.; Nam, C.H. (in press).
[75] Schroeder, H.; Chin, S.L. *Opt. Commun.* **2004,** *234,* 399–406.
[76] Schroeder, H.; Liu, J.; Chin, S.L. *Opt. Express* **2004,** *12,* 4768–4774.
[77] Méchain, G.; Couairon, A.; Franco, M.; Prade, B.; Mysyrowicz, A. *Phys. Rev. Lett.* **2004,** *93,* 035003-1–4.
[78] Liu, J.; Schroeder, H.; Chin, S.L.; Li, R.; Xu, Z. *Appl. Phys. Lett.* **2005,** *87,* 161105–161101-161103.
[79] Roskey, D.E.; Kolesik, M.; Moloney, J.V.; Wright, E.M. *Appl. Phys. B* **2007,** *86,* 249–258.
[80] Grow, T.D.; Ishaaya, A.A.; Vuong, L.T.; Gaeta, A.L.; Gavish, N.; Fibich, G. *Opt. Express* **2006,** *14,* 5468–5475.
[81] Pfeifer, T.; Gallmann, L.; Abel, M.J.; Neumark, D.M.; Leone, S.R. *Opt. Lett.* **2006,** *31,* 2326–2328.
[82] Kolesik, M.; Wright, E.M.; Becker, A.; Moloney, J.V. *Appl. Phys. B* **2006,** *85,* 531–538.
[83] Aumiler, D.; Ban, T.; Pichler, G. *Phys. Rev. A* **2005,** *71,* 063803-1–6.
[84] Brabec, T.; Krausz, F. *Phys. Rev. Lett.* **1997,** *78,* 3282–3285.
[85] Mlejnek, M.; Wright, E.M.; Moloney, J.V. *Phys. Rev. E* **1998,** *58,* 4903–4910.
[86] Zheltikov, A.M. *Phys. Rev. A* **2005,** *72,* 043812-1–4.
[87] Méjean, G.; Kasparian, J.; Yu, J.; Frey, S.; Salmon, E.; Ackerman, R.; Wolf, J.P.; Bergé, L.; Skupin, S. *Appl. Phys. B* **2006,** *82,* 341–345.
[88] Oberthaler, M.; Höpfl, R.A. *Appl. Phys. Lett.* **1993,** *63,* 1017–1019.
[89] Planas, S.A.; Pires Mansur, N.L.; Brito Cruz, C.H.; Fragnito, H.L. *Opt. Lett.* **1993,** *18,* 699–701.
[90] Washburn, B.R.; Buck, J.A.; Ralph, S.E. *Opt. Lett.* **2000,** *25,* 445–447.
[91] Liu, J.; Chen, X.; Liu, J.; Zhu, Y.; Leng, Y.; Dai, J.; Li, R.; Xu, Z. *Opt. Express* **2006,** *14,* 979–987.
[92] Bergé, L.; Rasmussen, J.J.; Kuznetsov, E.A.; Shapiro, E.G.; Turitsyn, S.K. *J. Opt. Soc. Am. B* **1996,** *13,* 1879–1891.
[93] Kasparian, J.; Sauerbrey, R.; Mondelain, D.; Niedermeier, S.; Yu, J.; Wolf, J.P.; André, Y.B.; Franco, M.; Prade, B.; Tzortzakis, S.; et al. *Opt. Lett.* **2000,** *25,* 1397–1399.
[94] Nuter, R.; Skupin, S.; Bergé, L. *Opt. Lett.* **2005,** *30,* 917–1399.
[95] Kandidov, V.P.; Kosareva, O.G.; Golubtsov, I.S.; Liu, W.; Becker, A.; Akózbek, N.; Bowden, C.M.; Chin, S.L. *Appl. Phys. B* **2003,** *77,* 149–165.
[96] Trushin, S.A.; Kosma, K.; Fuß, W.; Schmid, W.E. Chem. Phys. DOI: 10.1016/j.chemphys.2007.09.057. Published Online: http:// (accessed Oct 10, 2007/www.sciencedirect.com).
[97] Kovalenko, S.A.; Dobryakov, A.L.; Ruthmann, J.; Ernsting, N.P. *Phys. Rev. A* **1999,** *59,* 2369–2384.
[98] Druzhinin, S.I.; Ernsting, N.P.; Kovalenko, S.A.; Pérez Lustres, L.; Senyushkina, T.A.; Zachariasse, K.A. *J. Phys. Chem. A* **2006,** *110,* 2955–2969.
[99] Uiterwaal, C.J.G.J.; Gebhardt, C.R.; Schröder, H.; Kompa, K.-L. *Eur. Phys. J. D* **2004,** *30,* 379–392.
[100] Schröder, H. Personal communication, 2007.
[101] Pearse, R.W.B.; Gaydon, A.G. *The Identification of Molecular Spectra;* Chapman and Hall: London, 1976.
[102] Lofthus, A.; Krupenie, P.H. *J. Phys. Chem. Ref. Data* **1977,** *6,* 113–307.

[103] Luo, Q.; Liu, W.; Chin, S.L. *Appl. Phys. B* **2003,** *76,* 337–340.
[104] Turner, D.W.; Baker, C.; Baker, A.D.; Brundle, C.R. *Molecular Photoelectron Spectroscopy;* Wiley-Interscience: London, 1970.
[105] Dotchin, L.W.; Chupp, E.L.; Pegg, D.J. *J. Chem. Phys.* **1972,** *59,* 3960–3970.
[106] Lee, L.C.; Judge, D.L. *J. Phys. B* **1973,** *6,* L121–L123.